Diversity Waveform Sets for Delay-Doppler Imaging

Jiann-Ching Guey, *Member, IEEE*, and Mark R. Bell, *Member, IEEE*

Abstract— **Properties of the ambiguity function and the uncertainty relation of Fourier transforms assert fundamental limitations on the ability of any single radar waveform of constrained time–bandwidth product to distinguish two or more targets closely spaced in both time-delay (range) and Doppler-shift (radial velocity). These same mechanisms place fundamental limits on the ability radar imaging systems to distinguish separate scatterers in delay and Doppler. In this paper, the problem of using multiple waveform sets to make enhanced discrimination delay-Doppler measurements is considered. While small coded waveform sets for enhanced discrimination delay-only measurement are known (e.g., the Golay sequences), these waveforms do not have good Doppler discrimination properties. The problem of designing multiple waveform sets for enhanced discrimination delay-Doppler measurement is investigated, and the *composite ambiguity function* (CAF) is introduced as a tool to measure the delay-Doppler discrimination characteristics of these waveform sets. The problem of designing optimal coded waveform sets under a time–bandwidth product constraint is considered, and explicit optimal phase, frequency, and joint phase–frequency coded waveform sets having constant amplitude are presented. Algorithms for the construction of such waveform sets of arbitrary size and practical implementation issues are also presented.**

Index Terms— **Ambiguity functions, coded waveforms, radar waveforms, signal theory, time–frequency resolution.**

I. Introduction

A pulse-echo delay-Doppler measurement system such as a radar or active sonar measures an environment of interest by illuminating it with electromagnetic or acoustic radiation. The illuminating field scattered by objects in the environment is collected by a receiver, which processes the scattered signal to determine the presence and scattering characteristics of the objects that scattered the illuminating field. Two primary attributes characterizing the echo return are the round-trip propagation delay and the change in the received waveform resulting from the Doppler effect. The Doppler effect induces a compression or dilation of the time axis as a result of radial target motion toward or away from the pulse-echo sensor. For narrowband signals normally encountered in radar and scatterer motion having constant radial velocity, this is well approximated by a shift in the scattered waveform's center or carrier frequency proportional to the carrier frequency and the closing radial velocity between the target and scatterer [1]. In this paper, we will concentrate our attention on narrowband waveforms for which this approximation is valid. For such radar and sonar systems, the time-delay and Doppler-shift associated with the return from a scatterer are used as primary coordinates or indices for characterizing the scattered return.

A radar or other pulse-echo delay-Doppler measurement system can be viewed as an imaging system that forms a delay-Doppler image of the illuminated environment. We can think of the individual delays and Doppler shifts associated with individual scatterers in the illuminated environment as specifying points in a two-dimensional image with coordinates of delay τ and Doppler frequency shift ν. When the received signal is processed by a matched filter matched to a replica of the transmitted waveform delayed by τ and shifted in frequency by ν, the resulting measurement problem is equivalent to imaging the reflectivity of the illuminated environment using an aperture that is a function of the illuminating waveform [2, Ch. 9], [3, p. 58]. In the narrowband case, which we will assume throughout this entire paper, the point-spread function of the aperture is determined by the *ambiguity function* of the transmitted waveform.

When we view a radar system as an imaging system, it becomes clear that its ability to distinguish or discriminate between scatterers in delay and Doppler is determined by its convolution kernel or point-spread function. We have some control in selecting this kernel, since it is the ambiguity function of the waveform we choose to transmit. However, some fairly strong constraints on the mathematical form of the ambiguity function prohibit us from obtaining the ideal imaging kernel—a delta function located at the origin of the (τ, ν)-plane. Hence it may not be possible to obtain the desired discrimination capability using a single-pulse echo measurement made with a single waveform.

We use the term *discrimination* to denote the ability of an imaging radar system to separate and discern the presence of separate scatterers in a delay-Doppler image, and note that the discrimination properties of such a system are determined by the point-spread function of the imaging system (the ambiguity function). While there is a relationship between discrimination and resolution, there is a distinct difference as well. When speaking of the delay-Doppler *resolution* of a radar system, one is usually referring to the ability of the system to separate two closely spaced scatterers, and the ability of a system to do this is determined by the main lobe of the ambiguity function. So strictly speaking, resolution is a function only of the main lobe of the imaging point-spread function. However,

Manuscript received January 18, 1995; revised July 31, 1997. The material in this paper was presented in part at the 1995 IEEE International Symposium on Information Theory, Whistler, BC, Canada, September 20, 1995.

J.-C. Guey was with the School of Electrical Engineering, Purdue University, West Lafayette, IN 47907-1285 USA. He is now with Ericsson Inc., Research Triangle Park, NC USA.

M. R. Bell is with the School of Electrical Engineering, Purdue University, West Lafayette, IN 47907-1285 USA.

Publisher Item Identifier S 0018-9448(98)03463-4.

in delay-Doppler imaging of a scattering environment, low sidelobes can be essential in order to differentiate between or distinguish between mainlobe and sidelobe returns. If the sidelobes are too large, a small scatterer being imaged in the presence of a much larger scatterer may not be distinguished or resolved because it is hidden in the sidelobes of the ambiguity function. This problem, dealing with the sidelobe behavior of the point-spread function in addition to the mainlobe behavior is sometimes called *waveform self-clutter* [4], but has also been called *resolution* or *resolvability* in the radar literature [2, Sec. IV-C]. However, in this paper we are focusing on sidelobe elimination in the imaging point-spread function. For this reason we will use the term *discrimination* rather than *resolution* so that there is no confusion.

When discussing the resolution of a radar imaging system, we must be careful to define our terminology. The resolution of an imaging system is usually characterized by the point-spread function of the imaging system, which includes the sidelobe behavior of the point-spread function in addition to the main lobe behavior. However, most often discussions on resolution—and especially radar resolution—focus on the ability to separate two closely spaced, isolated targets, and the ability of a waveform to do this is determined by the width of the main lobe of its ambiguity function.

Viewing a radar system as a delay-Doppler imaging system that is the mathematical analog of an optical imaging system suggests a way around the delay-Doppler discrimination limitations of a single waveform measurement. In optical imaging and image processing, a number of investigators have considered the problem of constructing a high-resolution image using a number of low-resolution imaging systems having sufficiently different point-spread functions [5]–[7]. The analogy between pulse-echo delay-Doppler measurements and optical imaging suggests that one way around this problem is to make multiple pulse-echo measurements using waveforms having sufficiently different ambiguity functions and then process and combine the individual waveform returns to form an enhanced discrimination delay-Doppler image. Such a waveform-diverse measurement technique would allow for increased capability to spatially discriminate among scatterers in radar imaging (where one coordinate is derived from delay and the other from Doppler shift).

In this paper, we consider the use of this waveform-diverse measurement technique for obtaining enhanced discrimination delay-Doppler radar images, and we investigate the problem of designing phase, frequency, and phase–frequency coded waveform sets for making these measurements. In Section II, the discrimination characteristics of conventional single-waveform radar are described, and a multiple-waveform model leading to enhanced imaging capability is proposed which leads to the introduction of the *composite ambiguity function* of a set of waveforms. In Section III, a fundamental theorem for composite ambiguity function is established. With this theorem serving as a general rule, various coding schemes are investigated in Section IV for the purpose of designing enhanced discrimination waveform sets for this diversity-waveform radar imaging technique. Finally, practical implementation issues are addressed in Section V.

II. Problem Description

We now consider how a pulse-echo delay-Doppler measurement can be viewed as an imaging problem. Let $s(t)$ be the baseband analytic signal transmitted by the radar system. After being demodulated down to baseband, the received signal due to a scatterer with round-trip delay τ_0 and Doppler frequency shift ν_0 is

$$r(t) = s(t-\tau_0)e^{j2\pi\nu_0 t}e^{j\phi}$$

where $e^{j\phi}$ is the phase shift in the received carrier due to the propagation delay τ_0; hence $\phi = 2\pi f_0\tau_0$. If we process this signal with a matched filter

$$h_{\tau,\nu}(t) = s^*(T-t+\tau)e^{-j2\pi\nu(T-t)}$$

matched to the signal

$$q(t) = s(t-\tau)e^{j2\pi\nu t}$$

and designed to maximize the signal output at time T, the matched filter output at time T is given by

$$\mathcal{O}_T(\tau,\nu) = e^{-j\phi}\chi_s(\tau-\tau_0,\nu-\nu_0). \tag{1}$$

Here $\chi_s(\tau,\nu)$ is the *ambiguity function* of $s(t)$ given by

$$\chi_s(\tau,\nu) = \int_{-\infty}^{\infty} s(t)s^*(t-\tau)e^{-j2\pi\nu t}\,dt.$$

Because $h_{\tau,\nu}(t)$ is a linear time-invariant filter, if $\mu(\tau,\nu)$ describes a continuous scattering density, the response of the matched filter $h_{\tau,\nu}(t)$ to this scattering density is

$$\mathcal{O}_T(\tau,\nu) = \int_{-\infty}^{\infty}\int_{-\infty}^{\infty}\gamma(t,v)\chi_s(\tau-t,\nu-v)\,dt\,dv \tag{2}$$

where

$$\gamma(\tau,\nu) = \mu(\tau,\nu)e^{-j2\pi f_0\tau}.$$

This is the two-dimensional convolution of $\gamma(\tau,\nu)$ with $\chi_s(\tau,\nu)$, and can be thought of as the image of $\gamma(\tau,\nu)$ obtained using an imaging aperture with point-spread function $\chi(\tau,\nu)$ [8, Ch. 4].

From this imaging analogy of the delay-Doppler measurement process, we see that an ideal radar signal for simultaneous discrimination in delay and Doppler should have an ambiguity function that is a two-dimensional Dirac delta function $\delta(\tau,\nu)$ centered at the origin of the (τ,ν)-plane. The fundamental properties of ambiguity functions preclude the existence of a waveform having such ideal ambiguity function. This being the case, the next best thing to do is search for waveforms that have ambiguity functions approximating this ideal—ambiguity functions with a thumbtack-like shape (i.e., a narrow central peak surrounded by a low-level pedestal). This ensures that the response to a mismatched filter is uniformly small. This general approach to designing a radar signal approximating this ideal has been studied by several investigators [2], [9]–[11]. However, the properties of ambiguity functions limit

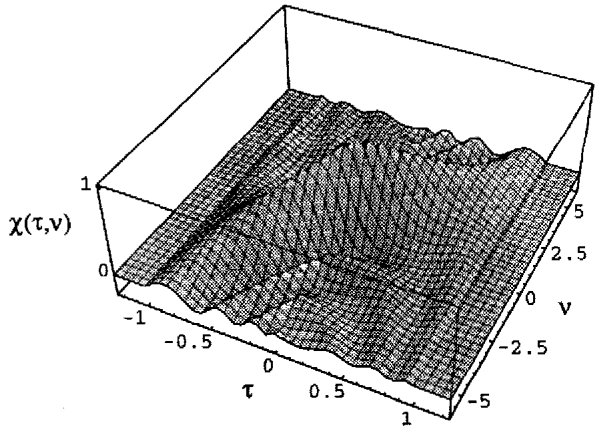

Fig. 1. Ambiguity function of a chirp waveform
$s(t) = \exp\{i\pi\alpha t^2\} I_{[-1/2,1/2]}(t)$
of duration 1 and $\alpha = 4$.

the degree to which such an ambiguity function can be approximated.

The viewpoint of a radar acting as an imaging system making a delay-Doppler image through an aperture whose point-spread function $\chi_s(\tau, \nu)$ is a function of the transmitted signal $s(t)$ is enlightening in terms of obtaining enhanced discrimination delay-Doppler images. We have some flexibility in selecting the point-spread function $\chi_s(\tau, \nu)$ through selection of the waveform $s(t)$. There are, however, some fairly strong restrictions on the form of the ambiguity function $\chi_s(\tau, \nu)$. In particular, the volume under its ambiguity surface[1] is given by

$$V_{\text{amb}} = \int_{-\infty}^{\infty}\int_{-\infty}^{\infty} |\chi_s(\tau, \nu)|^2 \, d\tau \, d\nu = \left| \int_{-\infty}^{\infty} |s(t)|^2 \, dt \right|^2$$

which is the energy in $s(t)$ squared. Therefore, for a fixed signal energy, the amount of ambiguity V_{amb} is fixed and cannot be reduced by modulating the signal, although doing so may redistribute the ambiguity in the (τ, ν)-plane. Also note that the ambiguity surface attains its maximum at $(\tau, \nu) = (0, 0)$ and

$$\chi_s(0, 0) = \int_{-\infty}^{\infty} s(t)s^*(t) \, dt = E.$$

These two properties and several others [2], [3] strongly constrain the set of two-dimensional functions that can be ambiguity surfaces. The volume under the surface must equal the square of the maximum. Any attempt to increase the peak height of the ambiguity function will result in increase in volume V_{amb} under the ambiguity surface. Furthermore, the uncertainty principle, which states that the product of mean-square duration $(\Delta t)^2$ and the mean-square bandwidth $(\Delta f)^2$ of the signal $s(t)$ must satisfy $(\Delta t)^2(\Delta f)^2 \geq 1/(4\pi)^2$ [12], [13], imposes the restrictions on simultaneously discriminating in both delay and Doppler. However, by correctly selecting a set of waveforms and then properly combining their individual matched-filter outputs, it is possible to bypass these constraints. The following example illustrates this.

[1] In general, the modulus squared of the ambiguity function is referred to as the *ambiguity surface*, while the volume under the ambiguity surface is referred to as the *amount of ambiguity* or simply the *ambiguity* of the signal.

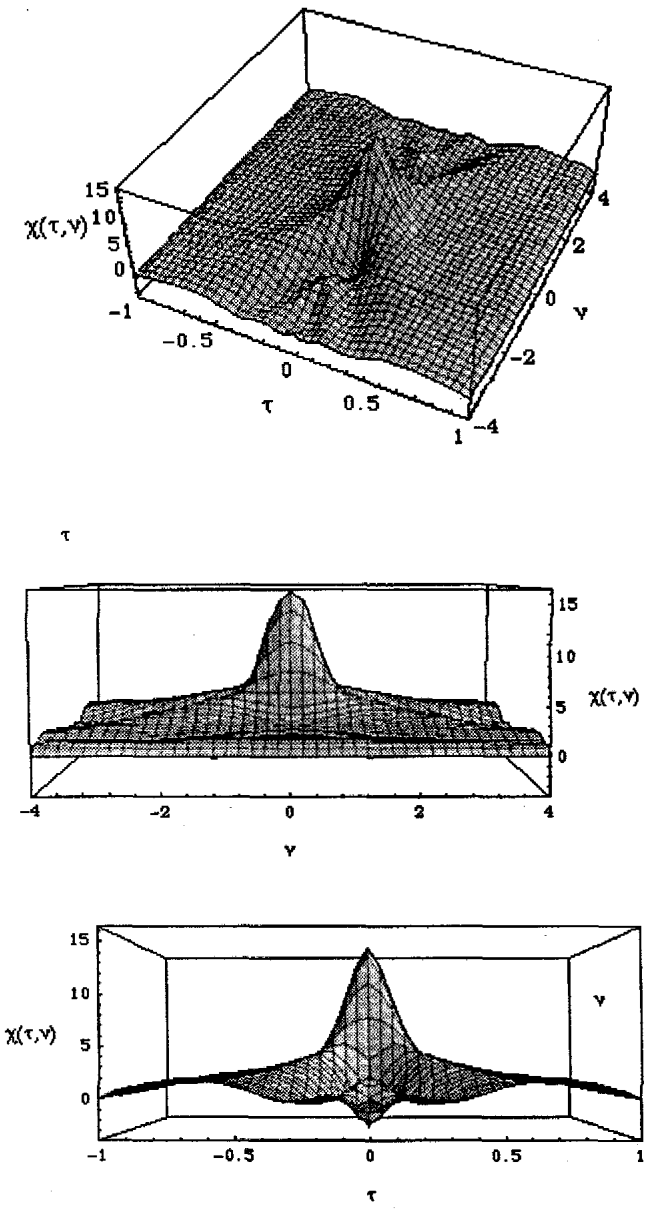

Fig. 2. Resulting ambiguity function from the coherent combination of the match filter outputs of 16 chirp waveforms
$s_j(t) = \exp\{i\pi\alpha_j t^2\} I_{[-1/2,1/2]}(t)$
of duration 1, with $\{\alpha_j\} = \{-8, \cdots, -1, 1, \cdots, 8\}$.

Fig. 1 shows the ambiguity function of a single chirp waveform $s(t) = \exp\{j\pi\alpha t^2\} \cdot 1_{[-T/2,T/2]}$ with duration $T = 1$ and parameter $\alpha = 4$. As can be seen from this figure, the overall delay-Doppler discrimination capabilities of a single-chirp waveform are not exceptionally good; strong returns can result from scatterers over a range of locations (τ, ν) about the line $\nu = \alpha\tau$. It is impossible to determine from a single measurement where, within this region, the scatterer is actually located. If, however, we transmit a number of chirp pulses $\{s_1(t), \cdots, s_K(t)\}$ of the form $s_k(t) = \exp\{j\pi\alpha_k t^2\} I_{[-1/2,1/2]}(t)$, each separated by a time interval of at least 1 (time unit), and process each using its respective matched filter and then coherently combine the matched filter outputs, the resulting ambiguity function (or output response) is as shown in Fig. 2, where 16 distinct chirp pulses were used.

Note that the resulting overall point-spread function is a great improvement over that of Fig. 1 for a single-chirp waveform if the goal is discrimination among scatterers in delay-Doppler imaging. Bernfeld [14] similarly showed that delay-Doppler resolution could be increased using multiple-chirp waveforms, although he used the inverse Radon transform to provide a tomographic reconstruction of the distribution of scatterers in delay and Doppler. This example only gives a qualitative result. The improvement can only be visually observed. To study quantitative aspects of this problem we will use an idealized mathematical model described as follows.

Consider an idealized situation in which a radar system is capable of operating simultaneously and independently on several independent channels. Each channel has its own transceiver and signal processor and is perfectly time-synchronized with the other channels. We also assume there is no crosstalk between channels. Hence, at the output of each channel we have a two-dimensional image of the target environment. For a point target located at (τ_0, ν_0), this can be formulated as

$$\begin{aligned}
\mathcal{O}_T^0(\tau, \nu) &= e^{j\phi} e^{-j2\pi(\nu-\nu_0)\tau_0} \chi_{s_0}(\tau - \tau_0, \nu - \nu_0) \\
&= \tilde{\chi}_{s_0}(\tau - \tau_0, \nu - \nu_0) \\
\mathcal{O}_T^1(\tau, \nu) &= e^{j\phi} e^{-j2\pi(\nu-\nu_0)\tau_0} \chi_{s_1}(\tau - \tau_0, \nu - \nu_0) \\
&= \tilde{\chi}_{s_1}(\tau - \tau_0, \nu - \nu_0) \\
&\vdots \quad \vdots \\
\mathcal{O}_T^{N-1}(\tau, \nu) &= e^{j\phi} e^{-j2\pi(\nu-\nu_0)\tau_0} \chi_{s_{N-1}}(\tau - \tau_0, \nu - \nu_0) \\
&= \tilde{\chi}_{s_{N-1}}(\tau - \tau_0, \nu - \nu_0) \qquad (3)
\end{aligned}$$

where $\mathcal{O}_T^i(\tau, \nu)$ is the image obtained through the ith channel and the notation $\tilde{\chi}$ is introduced to incorporate the complex modulation factor $e^{j\phi} e^{-j2\pi(\nu-\nu_0)\tau_0}$ into the ambiguity function. Coherently summing the images up gives a composite image

$$\mathcal{O}_T^C(\tau, \nu) = e^{j\phi} e^{-j2\pi(\nu-\nu_0)\tau_0} \sum_{i=0}^{N-1} \chi_{s_i}(\tau - \tau_0, \nu - \nu_0) \quad (4)$$

which can be thought of as an image of a point target generated by a new point-spread function

$$C(\tau, \nu) = \sum_{i=0}^{N-1} \chi_{s_i}(\tau, \nu). \quad (5)$$

This new point-spread function will be called the *composite ambiguity function* (CAF) or *combined ambiguity function*, as has been used in [4], to distinguish it from the ambiguity function of a single signal.

The key limitation in implementing this multiple-waveform delay-Doppler imaging scheme is the ability to get several independent noninterfereing measurements of the target environment at a particular point in time, or else be able to estimate and compensate for scatterer motion if the measurements are made in time sequentially. In situations where the target environment repeats periodically—for example, in some radar astronomy or radar imaging problems where there is sufficient control of the radar-target trajectory—this would be straightforward. In most applications, this will not be the case, and the channels need to be separated either in time or frequency domain. This will sometimes invalidate the assumption that the N radar images can be coherently combined in the manner described in (4), because in different time or frequency channels, the complex envelopes $e^{j\phi} e^{-j2\pi(\nu-\nu_0)\tau_0}$ that modulate the ambiguity functions may be different and cannot be accounted for to unwrap their effects on the individual images before they can be coherently combined. The implementation methods of realizing the method of coherent combining were briefly mentioned in [4]. An extensive discussion in the correspondences that followed [15], [16] lead to no apparent conclusion. In Section V, we propose an algorithm to approximate the coherent combining given in (4). For our theoretical interests, we will assume that (4) can be realized for the rest of the paper.

We will now study the composite ambiguity function and its use in the design of signal sets having improved delay-Doppler discrimination capabilities over single waveforms. Intuition suggests that we select the waveforms in our diversity waveform set so they have ambiguity functions that are in some sense as different as possible. In this way, there will be unique information in each individual waveform measurement. Alternatively, we can adopt the point of view that we wish to select waveforms that have the property that, with proper coherent combining of the filter outputs, large sidelobes in the ambiguity function can be canceled. In Section III, we will show that this intuition is indeed true if we measure the diversity among signals as the $\mathcal{L}_2$ distance between their ambiguity functions. In addition, by establishing the main theorem of CAF, we will show that waveform-diverse multiple measurements can improve radar discrimination significantly by reducing the amount of ambiguity of a point-spread function. In Section IV, we will investigate various coded waveform sets that have nice CAF properties. Since the signals used in each channel are different, we will have more flexibility in shaping the point-spread functions.

III. Main Theorem on Composite Ambiguity Function

We now consider the composite ambiguity function and its properties.

Definition 1: The **composite ambiguity function** (CAF) of a set of waveforms $\{s_0(t), s_1(t), \cdots, s_{K-1}(t)\}$ is defined as

$$C(\tau, \nu) = \sum_{i=0}^{K-1} \chi_{s_i}(\tau, \nu)$$

where χ_{s_i} is the ambiguity function of $s_i(t)$, $i = 0, 1, \cdots, K-1$.

The following theorem provides upper and lower bounds on the volume under a composite ambiguity surface and gives the conditions under which the lower bound is achieved.

Theorem 1: For a set of signals $\{s_0(t), s_1(t), \cdots, s_{K-1}(t)\}$ with total energy

$$E_T = \sum_{i=0}^{K-1} \int_{-\infty}^{\infty} |s_i(t)|^2 dt$$

define the volume $V_{\text{amb}}^{(c)}$ under their associated composite ambiguity function $C(\tau, \nu)$ as

$$V_{\text{amb}}^{(c)} = \int_{-\infty}^{\infty}\int_{-\infty}^{\infty} \left|\sum_{i=0}^{K-1} \chi_{s_i}(\tau, \nu)\right|^2 d\tau\, d\nu.$$

Then

1) The volume $V_{\text{amb}}^{(c)}$ satisfies

$$\frac{E_T^2}{K} \le V_{\text{amb}}^{(c)} = \sum_{i=0}^{K-1}\sum_{j=0}^{K-1} \left|\int_{-\infty}^{\infty} s_i(t)s_j^*(t)\, dt\right|^2 \le E_T^2.$$

2) Furthermore, the minimum is achieved when $\{s_0(t), s_1(t), \cdots, s_{K-1}(t)\}$ is a set of equal-energy orthogonal signals.

To prove this theorem, we need the following lemma.

Lemma 1: Given any two signals $s_i(t)$ and $s_j(t)$ of finite energy and their associate ambiguity functions $\chi_{s_i}(\tau, \nu)$ and $\chi_{s_j}(\tau, \nu)$, then

$$\begin{aligned}&\int_{-\infty}^{\infty}\int_{-\infty}^{\infty} \chi_{s_i}(\tau, \nu)\chi_{s_j}^*(\tau, \nu)\, d\tau\, d\nu \\ &\quad = \int_{-\infty}^{\infty}\int_{-\infty}^{\infty} \chi_{s_j}(\tau, \nu)\chi_{s_i}^*(\tau, \nu)\, d\tau\, d\nu \\ &\quad = \left|\int_{-\infty}^{\infty} s_i(t)s_j^*(t)\, dt\right|^2.\end{aligned}$$

Proof:

$$\begin{aligned}&\int_{-\infty}^{\infty}\int_{-\infty}^{\infty} \chi_{s_i}(\tau, \nu)\chi_{s_j}^*(\tau, \nu)\, d\tau\, d\nu \\ &= \int_{-\infty}^{\infty}\int_{-\infty}^{\infty}\int_{-\infty}^{\infty} s_i(t)s_i^*(t-\tau)e^{-j2\pi\nu t}\, dt \\ &\quad \cdot \int_{-\infty}^{\infty} s_j^*(u)s_j(u-\tau)e^{j2\pi\nu u}\, du\, d\tau\, d\nu \\ &= \int_{-\infty}^{\infty}\int_{-\infty}^{\infty}\int_{-\infty}^{\infty} s_i(t)s_i^*(t-\tau)s_j^*(u)s_j(u-\tau) \\ &\quad \cdot \int_{-\infty}^{\infty} e^{-j2\pi\nu(t-u)}\, d\nu\, dt\, du\, d\tau \\ &= \int_{-\infty}^{\infty}\int_{-\infty}^{\infty}\int_{-\infty}^{\infty} s_i(t)s_i^*(t-\tau)s_j^*(u)s_j(u-\tau) \\ &\quad \cdot \delta(t-u)\, dt\, du\, d\tau \\ &= \int_{-\infty}^{\infty}\int_{-\infty}^{\infty} s_i(u)s_i^*(u-\tau)s_j^*(u)s_j(u-\tau)\, du\, d\tau \\ &= \left|\int_{-\infty}^{\infty} s_i(t)s_j^*(t)\, dt\right|^2 \\ &= \int_{-\infty}^{\infty}\int_{-\infty}^{\infty} \chi_{s_j}(\tau, \nu)\chi_{s_i}^*(\tau, \nu)\, d\tau\, d\nu.\end{aligned}$$

Proof of Theorem 1:

i) Right inequality:

$$\begin{aligned}V_{\text{amb}}^{(c)} &= \int_{-\infty}^{\infty}\int_{-\infty}^{\infty} \left|\sum_{i=0}^{K-1} \chi_{s_i}(\tau, \nu)\right|^2 d\tau\, d\nu \\ &= \sum_{i=0}^{K-1}\sum_{j=0}^{K-1} \int_{-\infty}^{\infty}\int_{-\infty}^{\infty} \chi_{s_i}(\tau, \nu)\chi_{s_j}^*(\tau, \nu)\, d\tau\, d\nu \\ &= \sum_{i=0}^{K-1}\sum_{j=0}^{K-1} \left|\int_{-\infty}^{\infty} s_i(t)s_j^*(t)\, dt\right|^2 \qquad \text{Lemma 1} \\ &\le \sum_{i=0}^{K-1}\sum_{j=0}^{K-1} \int_{-\infty}^{\infty} |s_i(t)|^2\, dt \int_{-\infty}^{\infty} |s_j(t)|^2\, dt \\ &\qquad\qquad \text{Schwarz Inequality} \\ &= \left(\sum_{i=0}^{K-1} \int_{-\infty}^{\infty} |s_i(t)|^2\, dt\right)^2 = E_T^2.\end{aligned}$$

ii) Left inequality:

$$\begin{aligned}V_{\text{amb}}^{(c)} &= \sum_{i=0}^{K-1}\sum_{j=0}^{K-1} \left|\int_{-\infty}^{\infty} s_i(t)s_j^*(t)\, dt\right|^2 \\ &= \sum_{i=0}^{K-1} \left|\int_{-\infty}^{\infty} |s_i(t)|^2\, dt\right|^2 \\ &\quad + \sum_{i=0}^{K-1}\sum_{\substack{j=0 \\ j\ne i}}^{K-1} \left|\int_{-\infty}^{\infty} s_i(t)s_j^*(t)\, dt\right|^2 \\ &\ge \sum_{i=0}^{K-1} \left|\int_{-\infty}^{\infty} |s_i(t)|^2\, dt\right|^2 \ge \frac{E_T^2}{K}.\end{aligned}$$

Equalities hold when the signal set is equal-energy and orthogonal. □

So for a given total available energy, a composite ambiguity function will never have more ambiguity than a single ambiguity function—that is, the volume under the composite ambiguity surface will never be greater than the volume under the ambiguity surface of any single waveform. Note also that by choosing orthogonal signals in our signal set, we can decrease the volume under its composite ambiguity surface. It is actually this property that allows us to remove the ambiguity of a point-spread function by means of waveform-diverse multiple-measurements technique. This theorem provides a general rule of selecting a signal set for waveform-diverse measurements. Together with phase and frequency coding, it enables us to design a point-spread function not only with distribution of interest to us but also with a small amount of ambiguity.

Observation: Consider the set of all ambiguity functions as a metric space having metric defined by the $\mathcal{L}_2$ norm

$$d(\chi_{s_1}, \chi_{s_2}) = \int_{-\infty}^{\infty}\int_{-\infty}^{\infty} |\chi_{s_1}(\tau, \nu) - \chi_{s_2}(\tau, \nu)|^2\, d\tau\, d\nu.$$

Then the distance between two ambiguity functions χ_{s_1} and χ_{s_2}

$$\begin{aligned} d(\chi_{s_1}, \chi_{s_2}) &= \int_{-\infty}^{\infty} |\chi_{s_1}(\tau, \nu) - \chi_{s_2}(\tau, \nu)|^2 \, d\tau \, d\nu \\ &= \int_{-\infty}^{\infty} |\chi_{s_1}(\tau, \nu)|^2 \, d\tau \, d\nu \\ &\quad + \int_{-\infty}^{\infty} |\chi_{s_2}(\tau, \nu)|^2 \, d\tau \, d\nu \\ &\quad - 2\mathrm{Re}\left\{ \int_{-\infty}^{\infty} \chi_{s_1}(\tau, \nu) \chi_{s_2}^*(\tau, \nu) \, d\tau \, d\nu \right\} \\ &= E_1^2 + E_2^2 - 2\left| \int_{-\infty}^{\infty} s_1(t) s_2^*(t) \, dt \right|^2 \end{aligned}$$

is maximized when $s_1(t)$ and $s_2(t)$ are orthogonal. If we measure the diversity between ambiguity functions using the $\mathcal{L}_2$ distance, Theorem 1 has justified our intuition of selecting our signals as diverse as possible so that more information can be obtained through the difference in the matched-filter ambiguity responses provided by the diversity of the signal set.

IV. Coded Waveforms Design

Theorem 1 serves as a general rule for selecting a set of signals for waveform-diverse multiple measurements. However, it does not provide a constructive method for doing so. A set of orthogonal signals may have a small composite ambiguity volume $V_{\text{amb}}^{(c)}$, but this ambiguity volume may be poorly distributed. To distribute the ambiguity so that the composite ambiguity surface has a sharp central peak and uniformly low delay-Doppler sidelobes, appropriate modulation schemes are necessary. In this section, we will investigate various phase- and frequency-coded modulation schemes that yield a composite ambiguity surface having these properties. We will study only coded waveforms, because these waveforms result in designs that can be easily implemented in real systems. Particular families of waveforms that are investigated include

1) phase-coded waveforms;
2) frequency-coded waveforms;
3) jointly phase- and frequency-coded waveforms.

Unless otherwise specified, the coded waveform set will contain K signals $\{s_0(t), s_1(t), \cdots, s_{K-1}(t)\}$, where each

$$s_i(t) = \sum_{n=0}^{N-1} \psi_{i,n}(t - nT) \exp\{j2\pi d_{i,n} t/T\} \exp\{j\phi_{i,n}\} \tag{6}$$

consists of a sequence of N baseband pulses of length T, each having finite energy. Each pulse in the sequence is modulated by an integral frequency-modulating index $d_{i,n}$ and a phase $\phi_{i,n}$ that can take on any real-number value. To specify the modulating frequency and phase patterns of our coded waveforms, we will use tables of the form of Table I. All omitted items in these tables are assumed to be zero. For example, if the frequency hopping pattern d_k is omitted, then all d_k's are zero and the signal is not frequency-modulated.

TABLE I
Coding Pattern for a Quadruple-Phase Complementary Set

n		0	1	2	3
$s_0(t)$	$\phi_{0,n}$	0	0	0	0
$s_1(t)$	$\phi_{1,n}$	0	$2\pi/4$	$4\pi/4$	$6\pi/4$
$s_2(t)$	$\phi_{2,n}$	0	$4\pi/4$	$8\pi/4$	$12\pi/4$
$s_3(t)$	$\phi_{3,n}$	0	$6\pi/4$	$12\pi/4$	$18\pi/4$
$d_{i,n} = 0, \psi_{i,n}(t) = P_T(t)$					

A. Composite Ambiguity Function of a Coded Waveform Set

The ambiguity function of the signal in (6) is

$$\begin{aligned} \chi_{s_i}(\tau, \nu) &= \int_{-\infty}^{\infty} s_i(t) s_i^*(t - \tau) e^{-j2\pi\nu t} \, dt \\ &= \sum_{n=0}^{N-1} \sum_{m=0}^{N-1} e^{j(\phi_{i,n} - \phi_{i,m})} e^{j2\pi(d_{i,m}/T)\tau} \\ &\quad \cdot \int_{-\infty}^{\infty} \psi_{i,n}(t - nT) \psi_{i,m}^*(t - mT - \tau) \\ &\quad \cdot e^{-j2\pi(\nu - (d_{i,n} - d_{i,m}/T))t} \, dt \\ &= \sum_{n=0}^{N-1} \sum_{m=0}^{N-1} e^{j(\phi_{i,n} - \phi_{i,m})} e^{j2\pi(d_{i,m}/T)\tau} e^{-j2\pi\nu nT} \\ &\quad \cdot \chi_{\psi_{i,n}\psi_{i,m}}\left(\tau - nT + mT, \nu - \frac{d_n}{T} + \frac{d_m}{T}\right) \\ &= \sum_{n=0}^{N-1} \sum_{m=0}^{N-1} e^{j(\phi_{i,n} - \phi_{i,m})} \chi_{n,m}^{(i)}(\tau, \nu) \end{aligned} \tag{7}$$

where $\chi_{\psi_n\psi_m}(\tau, \nu)$ is the cross ambiguity function between $\psi_n(t)$ and $\psi_m(t)$, defined as

$$\chi_{\psi_n\psi_m}(\tau, \nu) = \int_{-\infty}^{\infty} \psi_n(t) \psi_m^*(t - \tau) e^{-j2\pi\nu t} \, dt$$

and

$$\begin{aligned} \chi_{n,m}^{(i)}(\tau, \nu) &= e^{j2\pi(d_{i,m}/T)\tau} e^{-j2\pi\nu nT} \\ &\quad \cdot \chi_{\psi_{i,n}\psi_{i,m}}\left(\tau - nT + mT, \nu - \frac{d_{i,n}}{T} + \frac{d_{i,m}}{T}\right). \end{aligned} \tag{8}$$

The composite ambiguity function of the signal set can be written as

$$\begin{aligned} C(\tau, \nu) &= \sum_{i=0}^{K-1} \sum_{n=0}^{N-1} \sum_{m=0}^{N-1} e^{j(\phi_{i,n} - \phi_{i,m})} \chi_{n,m}^{(i)}(\tau, \nu) \\ &= \sum_{i=0}^{K-1} \sum_{n=0}^{N-1} \chi_{n,n}^{(i)}(\tau, \nu) \\ &\quad + \sum_{i=0}^{K-1} \sum_{n=0}^{N-1} \sum_{\substack{m=0 \\ m \neq n}}^{N-1} e^{j(\phi_{i,n} - \phi_{i,m})} \chi_{n,m}^{(i)}(\tau, \nu). \end{aligned} \tag{9}$$

Note that we have decomposed the CAF into self-ambiguity and cross-ambiguity terms. Thus $C(\tau, \nu)$ is the superposition of N auto-ambiguity functions (sidelobes) located at the

origin and $N \times (N-1)$ cross-ambiguity functions located at $((n-m)T, (d_{i,n}-d_{i,m})/T)$ on the delay-Doppler plane. Furthermore, each of the cross-ambiguity function carries a complex phase factor $e^{j(\phi_n-\phi_m)}$. By appropriately designing the waveforms in a waveform set such that the locations and phases of the cross-ambiguity terms in (9) result in significant cross-term cancellation, we can design radar signal sets that provide substantial improvement in delay-Doppler discrimination.

B. Phase-Modulated Codes and Their Composite Ambiguity Functions

Perhaps the most well known family of phase-coded waveforms for the purpose of enhanced discrimination range measurements are the complementary sequences introduced by Golay [17]. These sequences are used to modulate the phase of the transmitted radar signal. A pair of binary complementary sequences have the property that if the two sequences are transmitted with a spacing longer than the length of each sequence, each sequence is processed with its corresponding matched filter, and the matched filter outputs are coherently added (after proper delay to account for the differing times of transmission), a cancellation of all sidelobes in the ambiguity function along the zero-Doppler axis occurs. Thus if we were interested in imaging scatterers of identical Doppler, a pair of complementary sequences provides an ideal set of pulse-echo waveforms. Other investigators have considered the properties of these sequences and related codes [18]–[21], and considered generalizations to sets that have more than a pair of signals [22] and polyphase complementary sequence sets [23]. Unfortunately, although the effective ambiguity functions of these complementary code sets have ideal properties along the zero-Doppler axis, off of the zero-Doppler axis they have many peaks, making unambiguous delay-Doppler imaging difficult.

Sivaswami [4] identified this problem and proposed the *subcomplementary* sets of sequences consisting of N sequences of length-N phase-modulated by a binary Hadamard matrix. The CAF of this sequence set has all its ambiguity sidelobes canceled. Instead of taking an *ad hoc* approach, in this section we derive a necessary and sufficient condition for a set of phase-modulated sequences to be "subcomplementary," as defined in [4], by exploiting Theorem 1.

If the coding patterns of the signal set are identical except for the phase-modulating indices $\phi_{i,j}$, then from (8) the $\chi^{(i)}_{n,m}$'s are identical. Thus from (9) (dropping the index i on $\chi^{(i)}_{n,m}$), the CAF of this signal set is

$$\begin{aligned} C(\tau,\nu) &= \sum_{i=0}^{K-1} \chi_{s_i}(\tau,\nu) \\ &= K \sum_{n=0}^{N-1} \chi_{n,n}(\tau,\nu) \\ &\quad + \sum_{n=0}^{N-1} \sum_{\substack{m=0 \\ m\neq n}}^{N-1} \chi_{n,m}(\tau,\nu) \sum_{i=0}^{K-1} e^{j(\phi_{i,n}-\phi_{i,m})}. \end{aligned} \tag{10}$$

If the phase coding patterns are selected such that

$$\sum_{i=0}^{K-1} e^{j(\phi_{i,n}-\phi_{i,m})} = 0, \qquad \text{for all } n \neq m$$

the second term in (10) vanishes and the sidelobes of the resulting CAF are completely canceled, leaving only the ambiguity functions of all individual pulses. In matrix form, this can be expressed as

$$\boldsymbol{\Phi}\boldsymbol{\Phi}^H = K\boldsymbol{I}_N \tag{11}$$

where

$$\boldsymbol{\Phi} = \begin{bmatrix} e^{j\phi_{0,0}} & e^{j\phi_{1,0}} & \cdots & e^{j\phi_{K-1,0}} \\ e^{j\phi_{0,1}} & e^{j\phi_{1,1}} & \cdots & e^{j\phi_{K-1,1}} \\ \vdots & \vdots & \ddots & \vdots \\ e^{j\phi_{0,N-1}} & e^{j\phi_{1,N-1}} & \cdots & e^{j\phi_{K-1,N-1}} \end{bmatrix}$$

is a matrix whose ith column is the phase-coding pattern of the ith signal, $\boldsymbol{\Phi}^H$ is its Hermitian transpose, and $\boldsymbol{I}_N$ is the $N \times N$ identity matrix.

For $N > K$, (11) has no solution, so we will consider the case of $N = K$. Solutions to (11) for $N = K$ will be referred to as *multiphase complementary sequences*. One of them, for arbitrary N, is

$$\phi_{i,n} = \frac{2\pi i n}{N}$$

for which

$$\sum_{i=0}^{N-1} e^{(j2\pi i/N)(n-m)} = 0, \qquad n \neq m.$$

Another solution can be constructed using Hadamard matrices. For example, for a set of two signals, the phase-modulating pattern can be

$$\boldsymbol{\Phi} = \boldsymbol{H}_1 = \begin{bmatrix} 1 & 1 \\ 1 & -1 \end{bmatrix}$$

for a set of 2^n signals, the modulating sequences can be obtained by using the expansion of a binary Hadamard matrix

$$\boldsymbol{H}_n = \begin{bmatrix} \boldsymbol{H}_{n-1} & \boldsymbol{H}_{n-1} \\ \boldsymbol{H}_{n-1} & -\boldsymbol{H}_{n-1} \end{bmatrix}.$$

The length of the sequences so constructed can only be powers of two. We can generalize this Hadamard matrix approach to waveform set construction. For example,

$$\tilde{\boldsymbol{H}}_1 = \begin{bmatrix} e^{j0} & e^{j0} & e^{j0} \\ e^{j0} & e^{j\frac{2\pi}{3}} & e^{j\frac{4\pi}{3}} \\ e^{j0} & e^{j\frac{4\pi}{3}} & e^{j\frac{8\pi}{3}} \end{bmatrix}$$

can be expanded by

$$\tilde{\boldsymbol{H}}_n = \begin{bmatrix} e^{j0}\tilde{\boldsymbol{H}}_{n-1} & e^{j0}\tilde{\boldsymbol{H}}_{n-1} & e^{j0}\tilde{\boldsymbol{H}}_{n-1} \\ e^{j0}\tilde{\boldsymbol{H}}_{n-1} & e^{j\frac{2\pi}{3}}\tilde{\boldsymbol{H}}_{n-1} & e^{j\frac{4\pi}{3}}\tilde{\boldsymbol{H}}_{n-1} \\ e^{j0}\tilde{\boldsymbol{H}}_{n-1} & e^{j\frac{4\pi}{3}}\tilde{\boldsymbol{H}}_{n-1} & e^{j\frac{8\pi}{3}}\tilde{\boldsymbol{H}}_{n-1} \end{bmatrix}.$$

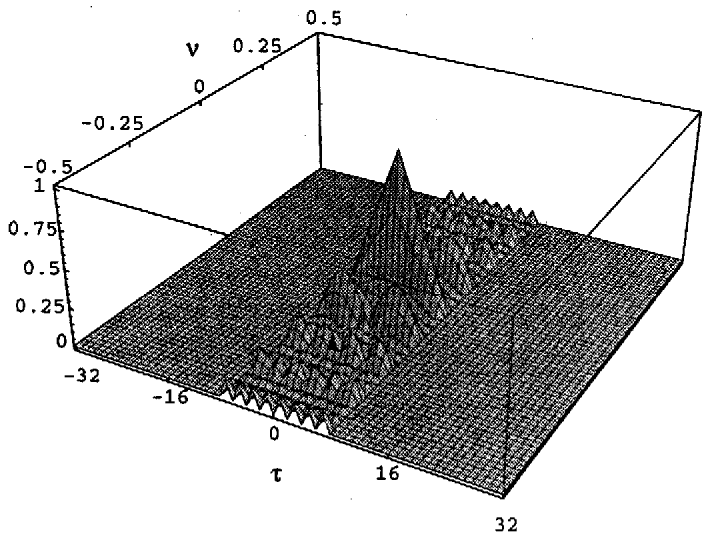

Fig. 3. CAF surface of signals in Table I, $T = 8$.

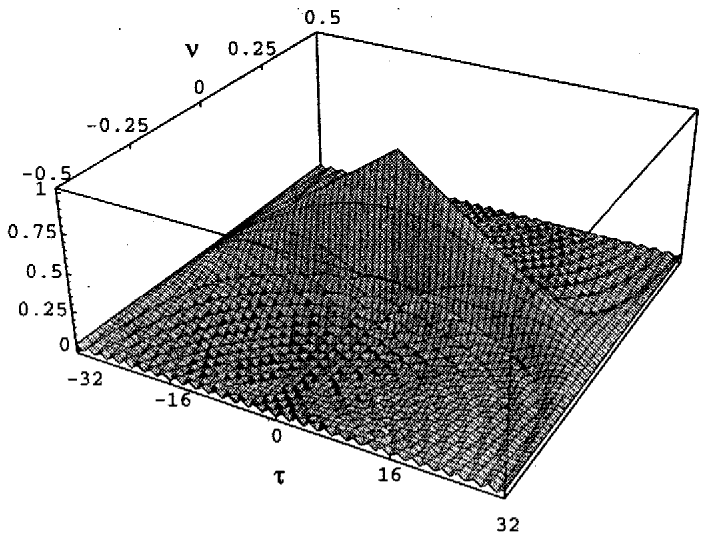

Fig. 4. Ambiguity surface of $s_0(t)$ in Table I, $T = 8$.

Moreover, if all $\phi_n(t)$'s have the same energy E, then the set is orthogonal, because for all $i \neq k$

$$\begin{aligned}\int_{-\infty}^{\infty} s_i(t)s_j^*(t)\,dt &= \int_{-\infty}^{\infty} \sum_{n=0}^{N-1} \psi_n(t-nT)e^{j\phi_{i,n}} \\ &\quad \cdot \sum_{m=0}^{N-1} \psi_m^*(t-mT)e^{-j\phi_{k,m}}\,dt \\ &= \sum_{n=0}^{N-1} e^{j(\phi_{i,n}-\phi_{k,n})} \\ &\quad \cdot \int_{nT}^{(n+1)T} |\psi_n(t-nT)|^2\,dt \\ &= E\sum_{n=0}^{N-1} e^{j(\phi_{i,n}-\phi_{k,n})} = 0.\end{aligned}$$

This follows from the fact that for $K = N$, $\mathbf{\Phi}\mathbf{\Phi}^H = NI_N$ if and only if $\mathbf{\Phi}^H\mathbf{\Phi} = NI_N$, which is true if and only if the rows of $\mathbf{\Phi}$ are orthogonal. Thus we see that if the set of N signals $\{s_0(t), \cdots, s_{N-1}(t)\}$ satisfies the following conditions:

1) $s_i(t) = \sum_{n=0}^{N-1} \psi_n(t-nT)e^{j\phi_{i,n}}$, $i = 0, 1, \cdots, N-1$,

2) $\int_{-\infty}^{\infty} |\psi_n(t)|^2\,dt = E$, for all $n = 0, 1, \cdots, N-1$,

3) $[\phi_{i,n}]$ is in the matrix form described above,

then its composite ambiguity function is

$$N\sum_{n=0}^{N-1} e^{-j2\pi\nu nT}\chi_{\psi_n}(\tau, \nu). \tag{12}$$

Furthermore, the set is an orthogonal set. Thus by Theorem 1, the multiphase complementary set is optimum in the sense of minimizing the volume under its CAF surface. Since the phase coding eliminates all of the sidelobes of the cross-ambiguity functions between different pulses and leaves only auto-ambiguity functions of all N individual pulses, (12) is exactly the CAF of the signal set

$$\{\sqrt{N}\psi_0(t), \sqrt{N}\psi_1(t-T), \cdots, \sqrt{N}\psi_{N-1}(t-(N-1)T)\}.$$

However, the multiphase complementary set has the advantage of having lower peak power, which is desirable in many radar applications.

An example of the multiphase complementary sequences of length 4 is given in Table I. Its associated CAF surface is plotted in Fig. 3. Compared to the ambiguity surface in Fig. 4 of $s_0(t)$, a single signal with length $4T$, its range discrimination is four times better while maintaining the same Doppler discrimination.

C. Frequency-Modulated Codes and Their Composite Ambiguity Functions

From (8), we know that the ambiguity sidelobe locations of a frequency-coded waveform are given by $((n-m)T, (d_{i,n}-d_{i,m})/T)$, which are completely determined by the frequency hopping pattern $d_{i,j}$. To study how the sidelobes are distributed on the (τ, ν)-plane, we construct the sidelobe matrix as a matrix whose i, jth entry contains the number of sidelobes located at $(iT, j/T)$. An example of a sidelobe distribution matrix is shown in Fig. 5. It corresponds to a frequency hopping sequence $\{0, 2, 5, 1, 3, 4\}$. Note that since the ambiguity function is odd-symmetric with respect to the zero-delay axis, it is actually sufficient to display only half of the matrix.

For a coded waveform of length N, there are $N \times (N-1)$ sidelobes that need to be allocated in the sidelobe matrix. A good frequency hopping pattern should then have a sidelobe matrix that contains no strong spikes other than the central peak and maintain a small signal bandwidth. Perhaps the most widely used frequency-modulated radar signal is the linear chirp $s(t) = \exp\{j\pi\alpha t^2\}$. It can be approximated by a linear stepped frequency-modulated signal with frequency-modulating pattern $d_0 = 0, d_1 = 1, \cdots, d_{N-1} = N-1$. If a thumbtack shape is considered optimal, then the linear frequency modulation (FM) is perhaps the worst possible frequency hopping waveform; its ambiguity function has a large ridge along the line of slope α in the (τ, ν)-plane. Costas [24] has suggested a new criterion for selection of frequency hopping pattern that yields ambiguity sidelobe matrix

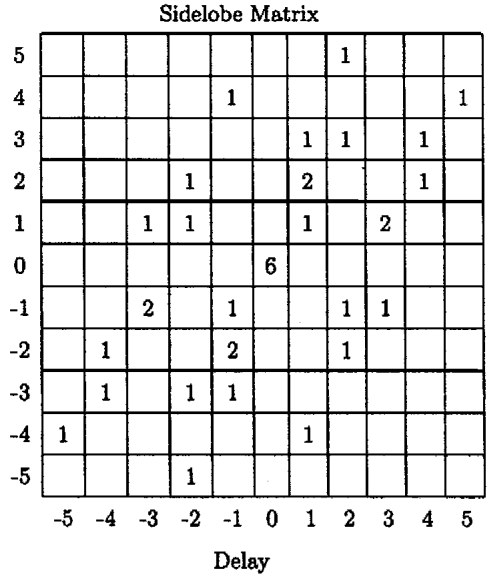

Fig. 5. Example of a sidelobe matrix.

approaching the ideal thumbtack shape. A Costas sequence of length N is a permutation of N consecutive integers that has a sidelobe distribution matrix containing only zero and one. Table II shows an example for Costas sequence of length 16. Its sidelobe matrix is given in Fig. 6. Our design of frequency hopping waveform set will be based on this particular category of signals.

A. Complementary Generalized Costas Pairs

To design a frequency-modulated code set for waveform-diversity multiple measurements, we can take a very long Costas sequence and break it into N equal-length subsequences. The sidelobe matrix of the resulting CAF is the summation of the sidelobe matrices of each individual sequence. For example, the Costas signal in Table II can be divided into three even pieces to form a set of signals in Table III. The sidelobe matrix of the resulting CAF is shown in Fig. 7. However, this is not an efficient way of allocating ambiguity on the (τ, ν)-plane since there are still many unoccupied spaces.

One way to solve this problem is to find a pair of equal-length Costas sequences that have complementary sidelobe distribution patterns. By coherently combining the ambiguity functions of these two signals, it is possible to increase the main lobe to sidelobe ratio by a factor of two without increasing the signal bandwidth. Unfortunately, it has been shown [25] that any two Costas signals of length N must have at least one common ambiguity sidelobe if $N > 3$. In this section, we introduce the idea of generalized Costas sequences and with a slightly increased signal bandwidth, we are able to find a pair of sequences that have complementary sidelobe distributions. In order to do this, we define the *distinct differences property* [26].

Definition 2: For integers M and N, let

$$I_M = \{0, 1, \cdots, M-1\}$$

and

$$I_N = \{0, 1, \cdots, N-1\}.$$

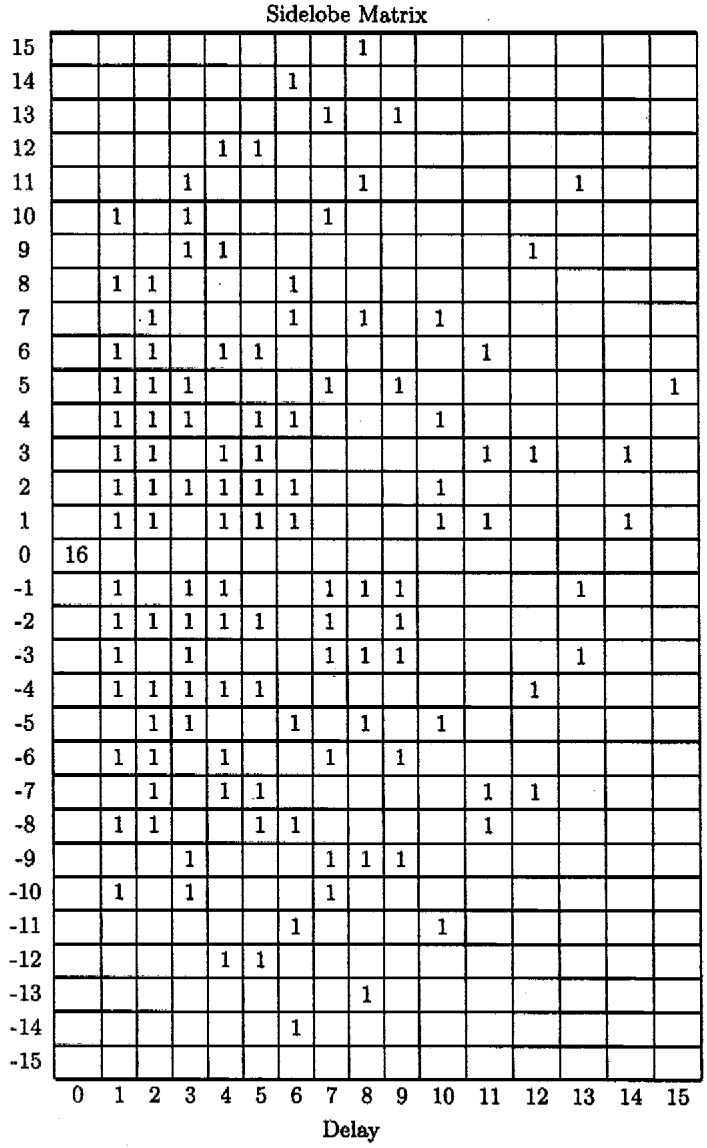

Fig. 6. Sidelobe matrix of the signal in Table II.

TABLE II
COSTAS SIGNAL OF LENGTH 16

n		0	1	2	3	4	5	6	7	8	9	10	11	12	13	14	15
$s(t)$	d_n	0	2	8	9	12	4	14	10	15	13	7	6	3	11	1	5
$d_n = 0, \psi_n(t) = P_T(t)$																	

A function $f: I_N \rightarrow I_M$ has the **distinct differences property** if

$$f(i+h) - f(i) = f(j+h) - f(j) \rightarrow i = j$$

for all integers h, i, and j, with $1 \leq h \leq N-1$ and $0 \leq i, j \leq N-h-1$.

A Costas sequence can then be thought of as a permutation $f: I_N \rightarrow I_N$ that satisfies the distinct differences property.

Definition 3: For $N \leq M$, we define the **generalized Costas sequence** as a mapping $f: I_N \rightarrow I_M$ with distinct differences property of I_N into one of the permutations of N distinct integers in I_M.

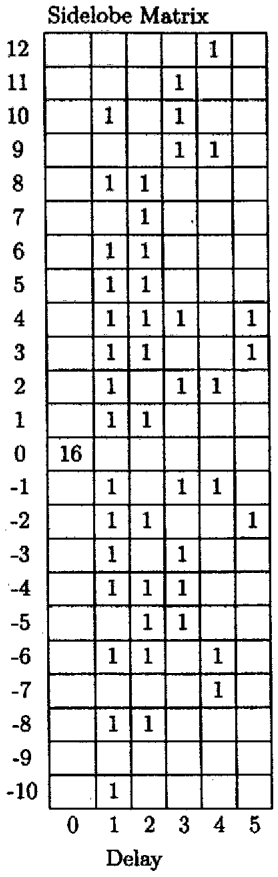

Fig. 7. Sidelobe matrix of the signal in Table III.

For example,

$$f(0)=0,\quad f(1)=1,\quad f(2)=6,\quad f(3)=3$$
$$f(4)=7,\quad f(5)=2,\quad f(6)=5$$

or simply $\{0, 1, 6, 3, 7, 2, 5\}$ is a generalized Costas sequence of f: $I_7 \rightarrow I_8$. Note that unlike a Costas sequence, the range of this function is not a set of consecutive integers. In the given example, the number 4 is not in the range.

It is obvious that the collection of Costas sequences of length N is a subset of the generalized Costas sequences of f: $I_N \rightarrow I_M$ for all $M \geq N$. Thus we have created a larger set in which we can search for pairs of sequences that have complementary sidelobes distributions. Table IV lists the number of generalized Costas sequence for f: $I_7 \rightarrow I_8$. The notation $I_8 - \{i\}$ indicates that the number i is left out in the range space. As expected, when 0 and 1 are left out, the number of generalized Costas sequences is 200, same as that of the Costas sequence of length 8. When 3 and 4 are left out, it increases to 572. With a slight increase of signal bandwidth, the available sequences with distinct differences property increases from 200 for normal Costas sequence to 3232 for generalized Costas sequence.

Exhaustive search is performed by checking if any sequence pair among all possible generalized Costas sequences in the mapping $I_N \rightarrow I_M$ satisfies the complementary condition. The results show that complementary generalized Costas pairs exist for f: $I_N \rightarrow I_{N+1}$ up to $N = 8$. For f: $I_N \rightarrow I_{N+2}$, they exist for N up to 10. The following are some examples.

TABLE III
THE BREAKDOWN OF A LONG COSTAS SEQUENCE

n		0	1	2	3	4	5
$s_0(t)$	$d_{0,n}$	0	2	8	9	12	4
$s_1(t)$	$d_{1,n}$	4	14	10	15	13	7
$s_2(t)$	$d_{2,n}$	7	6	3	11	1	5

TABLE IV
NUMBER OF GENERALIZED COSTAS SEQUENCES FOR f: $I_7 \rightarrow I_8$

	I_8 $-\{0\}$	I_8 $-\{1\}$	I_8 $-\{2\}$	I_8 $-\{3\}$	I_8 $-\{4\}$	I_8 $-\{5\}$	I_8 $-\{6\}$	I_8 $-\{7\}$	total
number of sequences	200	364	480	572	572	480	364	200	3232

1) f: $I_7 \rightarrow I_8$, a total of 16 pairs have been found, one of which is

$$\begin{Bmatrix} 1 & 4 & 3 & 7 & 2 & 0 & 6 \\ 6 & 0 & 2 & 7 & 3 & 4 & 1 \end{Bmatrix}.$$

2) f: $I_8 \rightarrow I_9$, four pairs have been found, one of which is

$$\begin{Bmatrix} 1 & 8 & 3 & 7 & 6 & 0 & 2 & 5 \\ 7 & 0 & 5 & 1 & 2 & 8 & 6 & 3 \end{Bmatrix}.$$

3) f: $I_9 \rightarrow I_{11}$, 32 pairs have been found, one of which is

$$\begin{Bmatrix} 2 & 3 & 9 & 6 & 4 & 0 & 8 & 1 & 10 \\ 10 & 1 & 8 & 0 & 4 & 6 & 9 & 3 & 2 \end{Bmatrix}.$$

4) f: $I_{10} \rightarrow I_{12}$, four pairs have been found, two of which are

$$\begin{Bmatrix} 7 & 3 & 1 & 0 & 9 & 4 & 11 & 5 & 2 & 10 \\ 4 & 8 & 10 & 11 & 2 & 7 & 0 & 6 & 9 & 1 \end{Bmatrix}.$$

$$\begin{Bmatrix} 7 & 3 & 1 & 0 & 9 & 4 & 11 & 5 & 2 & 10 \\ 10 & 2 & 5 & 11 & 4 & 9 & 0 & 1 & 3 & 7 \end{Bmatrix}.$$

These results are summarized in Table V. For a mapping in which a complementary Costas pair exists, the maximum achievable peak to sidelobe ratio is $2N : 1$. The cost of using sequences in a bigger set is a slight increase in signal bandwidth. A good indication of the bandwidth-efficient signal design is therefore the ratio between the peak-to-sidelobe ratio to the highest frequency component (i.e., M) in the signal set. This value is always one for a single Costas sequence. For a complementary generalized Costas pair found in the mapping $I_7 \rightarrow I_8$, this ratio is $(14 : 1)/8$.

A complementary generalized Costas pair can be further divided into a larger set of shorter complementary sequences. For example,

$$\begin{Bmatrix} 1 & 4 & 3 & 7 & 2 & 0 & 6 \\ 6 & 0 & 2 & 7 & 3 & 4 & 1 \end{Bmatrix}$$

can be divided into a set of four sequences

$$\begin{Bmatrix} 1 & 4 & 3 & 7 \\ 7 & 2 & 0 & 6 \\ 6 & 0 & 2 & 7 \\ 7 & 3 & 4 & 1 \end{Bmatrix}. \tag{13}$$

TABLE V
SUMMARY OF EXHAUSTIVE SEARCH

	highest freq. component	number of generalized Costas sequences	number of complementary pairs	max. peak to sidelobe ratio
$I_7 \rightarrow I_8$	8	3232	16	14:1
$I_8 \rightarrow I_9$	9	9860	4	16:1
$I_9 \rightarrow I_{10}$	10	28968	0	9:1
$I_9 \rightarrow I_{11}$	11	328756	32	18:1
$I_{10} \rightarrow I_{11}$	11	82116	0	10:1
$I_{10} \rightarrow I_{12}$	12	1151904	4	20:1

TABLE VI
COMPLEMENTARY GENERALIZED COSTAS PAIR OF LENGTH 8

n		1	2	3	4	5	6	7	8
$s_0(t)$	$d_{0,n}$	1	8	3	7	6	0	2	5
$s_1(t)$	$d_{1,n}$	7	0	5	1	2	8	6	3
$\psi_{i,n}(t) = P_T(t)$ for all i and n									

The sidelobe matrix of the resulting composite ambiguity function for these four sequences is given in Fig. 8. The columns right next to the zero-delay column are almost full. Compared with the sidelobe matrix of a single Costas sequence, this is a much more efficient way of allocating ambiguity. Note that complementary triplets or higher order sets also exist. A trivial example for a triplet is to divide the length-16 Costas sequence given in Table II into three subsequences: $\{0, 2, 8, 9, 12, 4\}$, $\{4, 14, 10, 15, 13, 7\}$, and $\{7, 6, 3, 11, 1, 5\}$, which can be further reduced to $\{0, 2, 8, 9, 12, 4\}$, $\{0, 10, 6, 11, 9, 3\}$, and $\{6, 5, 2, 10, 0, 4\}$. It is obvious that they are a complementary triplet of $I_6 \rightarrow I_{13}$. However, we are not sure if I_{13} is the smallest range in which a complementary triplet of length 6 exists. An exhaustive search process of such triplets is very time-consuming and, therefore, was not attempted in this study.

To demonstrate the improvement in peak-to-sidelobe ratio over a single Costas waveform, a pair of complementary generalized Costas sequences are used to modulate the waveform set in Table VI. Its CAF surface is plotted in Fig. 9. The ambiguity surface of $s_0(t)$ in the same table is plotted in Fig. 10 for comparison. Several cross cuts along fixed delays of these two ambiguity surfaces are plotted in Figs. 11–16. The lower peak-to-sidelobe ratio and smaller amount of ambiguity reveal the advantage of using waveform-diverse multiple measurements.

B. Circular Costas Signal Set

In Theorem 1, we showed that the minimum achievable volume of a composite ambiguity surface is the total energy of the signal set squared divided by the number of signals. Thus a pair of signals can only reduce the ambiguity volume $V_{\text{amb}}^{(c)}$ to half that of a single signal at most. To further reduce the volume of the point-spread function, we need a larger set. Theorem 1 also states that the minimum is attained when the set is orthogonal and equal-energy. An arbitrary set of frequency-modulated orthogonal signals may have a very small amount of composite ambiguity, but it may not have the desired distribution, i.e., the thumbtack-like shape. On the other hand, if we pick any N signals that have nice distribution properties (e.g., N equal-length Costas signals), they may not be orthogonal.

7		1				1	
6	1		1		1		1
5			1		1		
4		1	1		1	1	
3		1	1		1	1	
2		1	1		1	1	
1	1		1		1		1
0				16			
-1	1		1		1		1
-2		1	1		1	1	
-3		1	1		1	1	
-4		1	1		1	1	
-5			1		1		
-6	1		1		1		1
-7		1				1	
	-3	-2	-1	0	1	2	3

Fig. 8. Sidelobe matrix of the signals in (13).

In this section we introduce the circular Costas signal set which is a collection of equal-length orthogonal Costas signals. The construction of this set requires the use of Welch construction method [27], [28] described below.

Consider the Galois field $\text{GF}(p)$ of prime order p with integer elements $\{0, 1, \cdots, p-1\}$ and integer arithmetic modulo p. Let g be a primitive root of $\text{GF}(p)$. Then the sequence $\{g, g^2, \cdots, g^{p-1}\} \pmod p$ is a Costas sequence of length $p-1$. Furthermore, every circular shift of the original sequence is a Costas sequence of length $p-1$. A Costas sequence with this property is said to be a *circular Costas sequence* [29].

For example, 3 is a primitive root modulo 7. Therefore, $\{3\,2\,6\,4\,5\,1\}$ is a Costas sequence; so are all its circular shifts. If we add together the sidelobe-distribution matrices of all six Costas sequences obtained by circular shifts of this original sequence, the resulting sidelobes will have a distribution as in Fig. 17. Note that the peak-to-sidelobe ratio decreases linearly

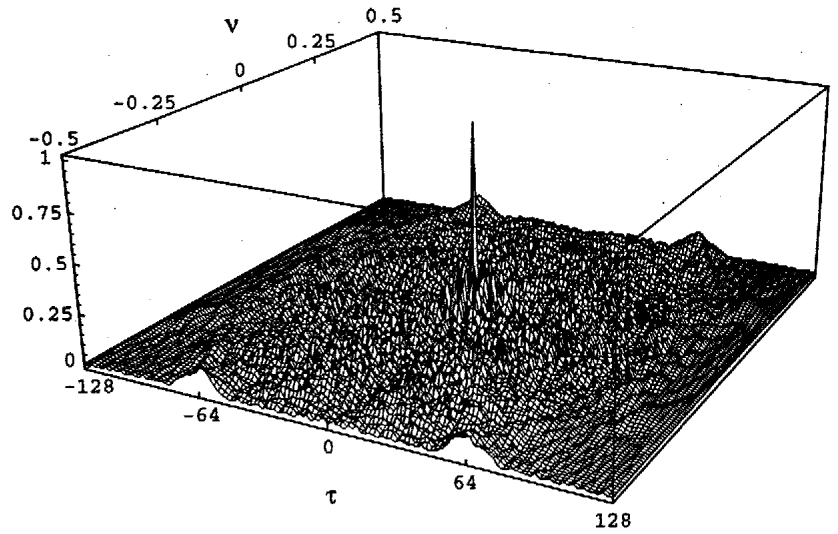

Fig. 9. CAF surface of signals in Table VI, $T = 16$.

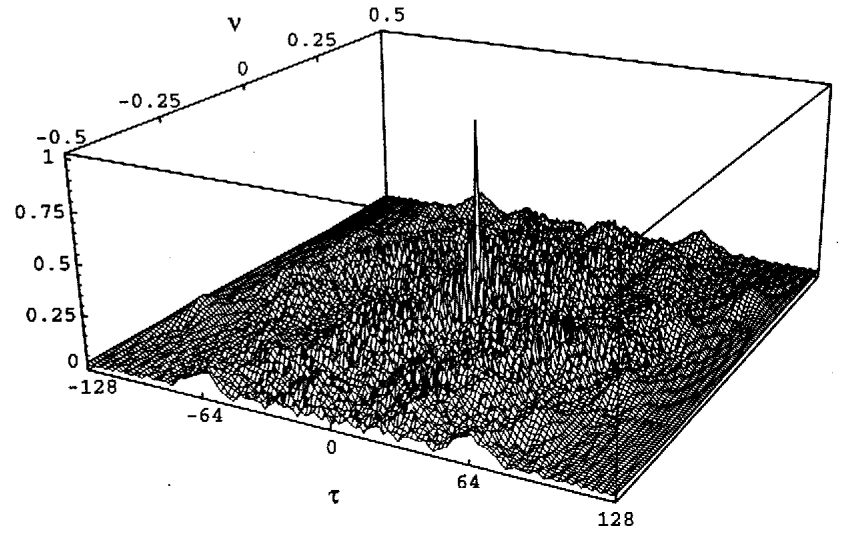

Fig. 10. Ambiguity surface of $s_0(t)$ in Table VI, $T = 16$.

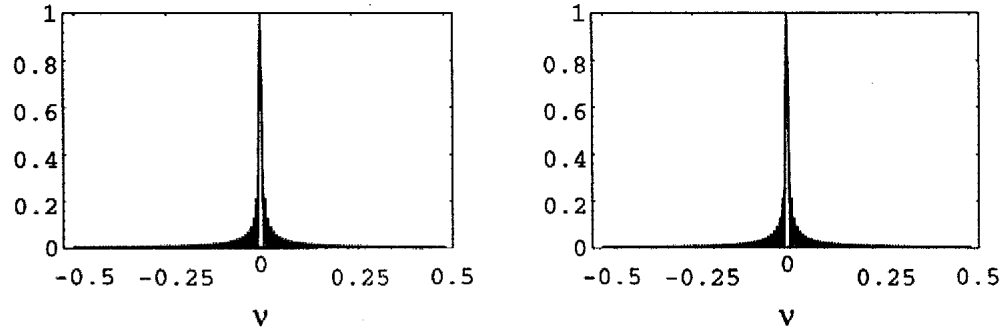

Fig. 11. Left: Cross cut of Fig. 10 at $\tau = 0$. Right: Cross cut of Fig. 9 at $\tau = 0$.

as the column index increases. In the last column, the peak-to-sidelobe ratio is 36 : 1 compared to 6 : 1 of a single Costas sequence of length 6. This code is used to modulate the frequency hopping pattern of the signal set in Table VII. Since $\psi_{i,n}(t) = P_T(t)$ for all i and n, where

$$P_T(t) = 1_{[0,T]}(t)$$

it is clear from the fact that

$$\int_0^T e^{[j2\pi(i-j)t/T]}\,dt = 0, \qquad \text{for } i \neq j$$

that the set is orthogonal, since each frequency is transmitted only once in each time slot. Thus we have a construction for an orthogonal signal set with the desired ambiguity properties.

The CAF surface of this signal set is plotted in Fig. 18. Compared with the ambiguity surface in Fig. 19 of a single Costas signal, its peak-to-sidelobe ratio decreases rapidly as τ increases as opposed to the constant value of a single Costas signal. This significant improvement is demonstrated by the plots (Figs. 20–25) of cross cuts along integral multiples of T of Figs. 18 and 19.

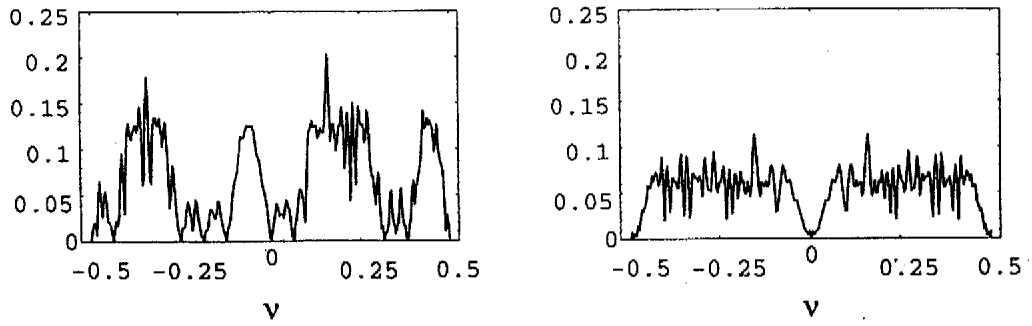

Fig. 12. Left: Cross cut of Fig. 10 at $\tau = T$. Right: Cross cut of Fig. 9 at $\tau = T$.

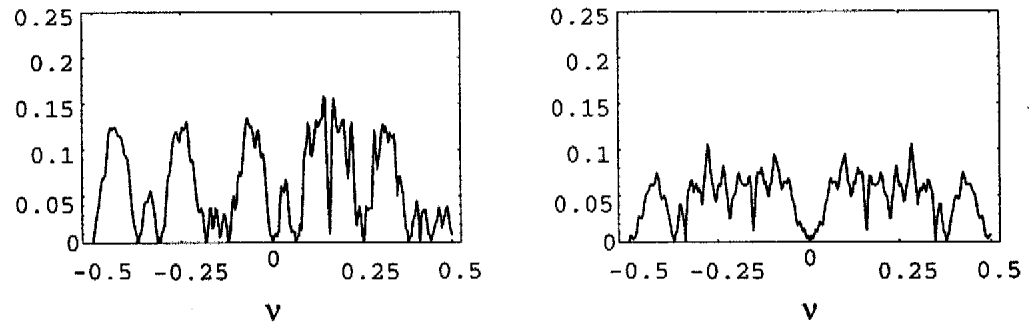

Fig. 13. Left: Cross cut of Fig. 10 at $\tau = 2T$. Right: Cross cut of Fig. 9 at $\tau = 2T$.

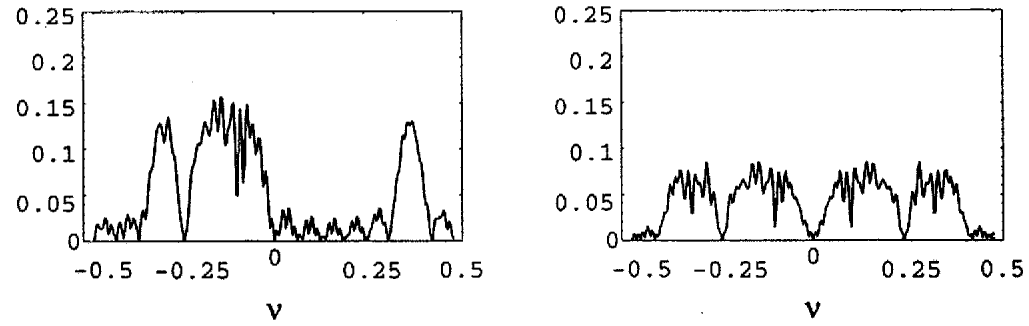

Fig. 14. Left: Cross cut of Fig. 10 at $\tau - 3T$. Right: Cross cut of Fig. 9 at $\tau = 3T$.

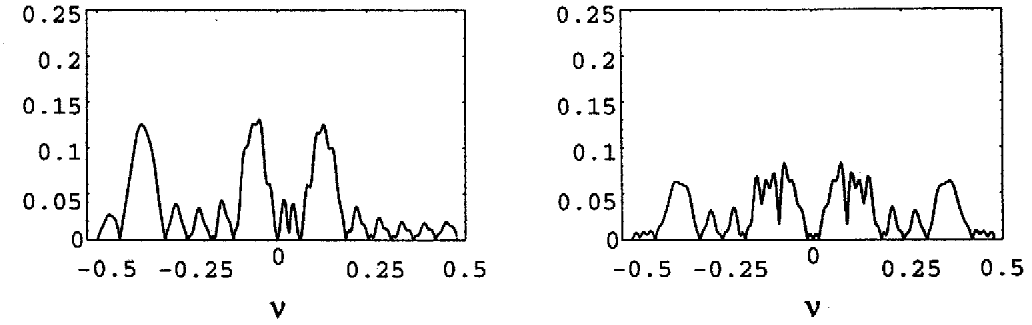

Fig. 15. Left: Cross cut of Fig. 10 at $\tau = 5T$. Right: Cross cut of Fig. 9 at $\tau = 5T$.

C. Mixed-Phase and Frequency-Modulated Codes and Their Composite Ambiguity Functions

In the example given in Table I, the baseband signal $\psi_n(t)$ is a rectangular pulse. Even though the signal set is optimal in the ambiguity volume sense because it is orthogonal, its composite ambiguity surface does not have the desired thumbtack shape. The composite ambiguity can be distributed more evenly if we are willing to frequency-modulate $\psi_n(t)$. The following is an example of applying both phase coding and frequency coding on a set of signals.

Consider a set of four signals $\{s_0(t), s_1(t), s_2(t), s_3(t)\}$, defined by

$$s_i(t) = \sum_{n=0}^{3} \Psi_n(t - 4nT) e^{j\Phi_{i,n}}$$

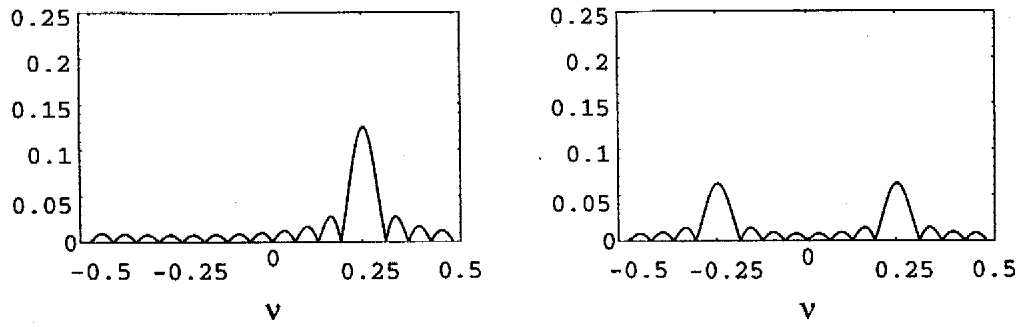

Fig. 16. Left: Cross cut of Fig. 10 at $\tau = 7T$. Right: Cross cut of Fig. 9 at $\tau = 7T$.

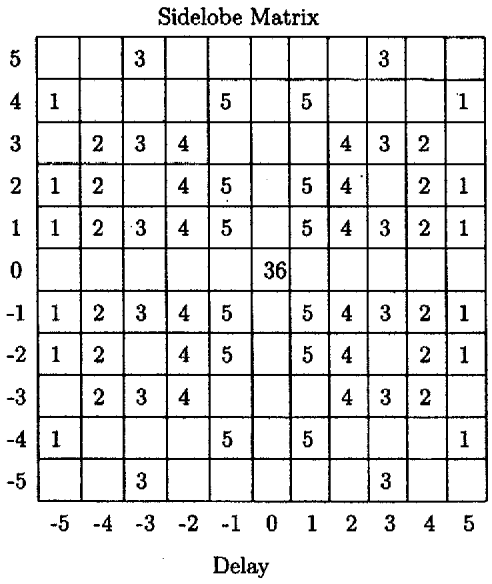

Fig. 17. Sidelobe matrix of a circular Costas sequences of length 6.

where $\Phi_{i,n}$ is coded by the quadruple-phase complementary code, i.e., $\Phi_{i,n} = 2\pi in/4$ and $\Psi_n(t)$'s are frequency-modulated by the hopping pattern given in (13)

$$\begin{aligned}\Psi_0(t) &= P_T(t)e^{\frac{j2\pi t}{T}} + P_T(t-T)e^{\frac{j2\pi 4t}{T}} \\ &\quad + P_T(t-2T)e^{\frac{j2\pi 3t}{T}} + P_T(t-3T)e^{\frac{j2\pi 7t}{T}} \\ \Psi_1(t) &= P_T(t)e^{\frac{j2\pi 7t}{T}} + P_T(t-T)e^{\frac{j2\pi 2t}{T}} \\ &\quad + P_T(t-2T) + P_T(t-3T)e^{\frac{j2\pi 6t}{T}} \\ \Psi_2(t) &= P_T(t)e^{\frac{j2\pi 6t}{T}} + P_T(t-T) \\ &\quad + P_T(t-2T)e^{\frac{j2\pi 2t}{T}} + P_T(t-3T)e^{\frac{j2\pi 7t}{T}} \\ \Psi_3(t) &= P_T(t)e^{\frac{j2\pi 7t}{T}} + P_T(t-T)e^{\frac{j2\pi 3t}{T}} \\ &\quad + P_T(t-2T)e^{\frac{j2\pi 4t}{T}} + P_T(t-3T)e^{\frac{j2\pi t}{T}}.\end{aligned}$$

Table VIII contains the overall coding pattern of this signal set if we express the signals in the form

$$s_i(t) = \sum_{n=0}^{15} \exp(j\phi_{i,n}) \exp(j2\pi d_{i,n}t/T)\psi_{i,n}(t-nT).$$

The $\Psi_n(t)$'s all have the same energy, and they are orthogonal, and from (12) their composite ambiguity function

TABLE VII
CIRCULAR COSTAS SEQUENCES OF LENGTH 6

n		0	1	2	3	4	5
$s_0(t)$	$d_{0,n}$	0	2	1	5	3	4
$s_1(t)$	$d_{1,n}$	2	1	5	3	4	0
$s_2(t)$	$d_{2,n}$	1	5	3	4	0	2
$s_3(t)$	$d_{3,n}$	5	3	4	0	2	1
$s_4(t)$	$d_{4,n}$	3	4	0	2	1	5
$s_5(t)$	$d_{5,n}$	4	0	2	1	5	3
$\psi_{i,n}(t) = P_T(t)$ for all i and n							

is

$$4\sum_{n=0}^{3} e^{-j2\pi\nu n4T}\chi_{\Psi_n}(\tau, \nu) \tag{14}$$

where $\chi_{\Psi_n}(\tau, \nu)$ is the auto-ambiguity function of $\Psi_n(t)$. Since $e^{-j2\pi\nu n4T}$ is one whenever ν is an integral multiple of $1/T$, the sidelobe distribution matrix of (14) remains the same as in Fig. 8. Thus we have constructed a set of signals whose composite ambiguity function has the following desirable ambiguity properties.

1) With highest frequency being $7/T$, it has a peak-to-sidelobe ratio of 16 : 1 that could have only been achieved by using a single Costas sequence of length 16 (i.e., a signal with highest frequency being $15/T$.)
2) It has total ambiguity $E_T^2/4$, which can only be achieved by a single signal with energy $E_T/2$.
3) It has zero ambiguity for $\tau > 4T$, which can only be achieved by a single signal with length less than $4T$.

The CAF surface of this signal set is plotted in Fig. 26. Also plotted in Fig. 27 is the ambiguity surface of the Costas sequence of length 16 in Table II for comparison. It is clear that the CAF surface of the signal set in Table VIII has significantly less ambiguity than the ambiguity surface of a Costas sequence of length 16. Moreover, the ambiguity of the Costas sequence spreads over the entire (τ, ν)-plane while the ambiguity of the coded waveform set is confined in the region $-128 < \tau < 128$ and $-0.25 < \nu < 0.25$. It is easy to generalize this construction technique to the design of waveform sets with larger sequence lengths n. Hence we have a general technique for the design of joint phase- and frequency-coded waveform sets having very good composite ambiguity behavior.

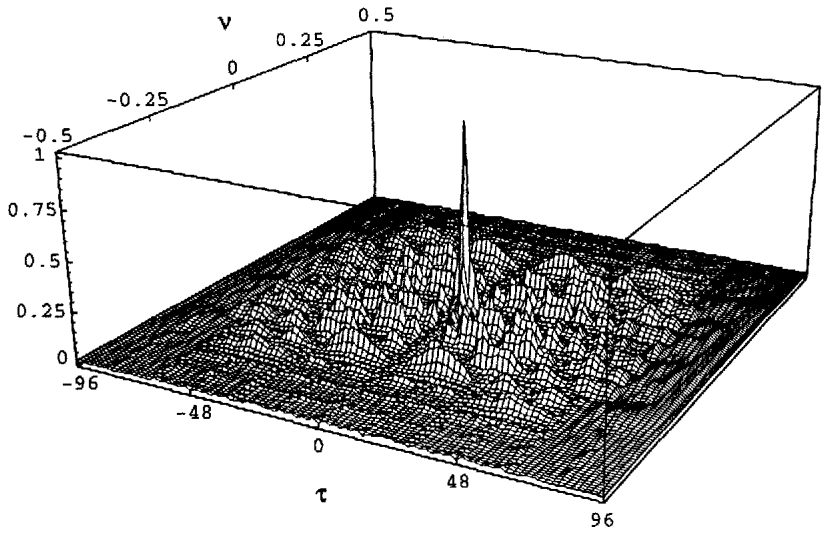

Fig. 18. CAF surface of signals in Table VII, $T = 16$.

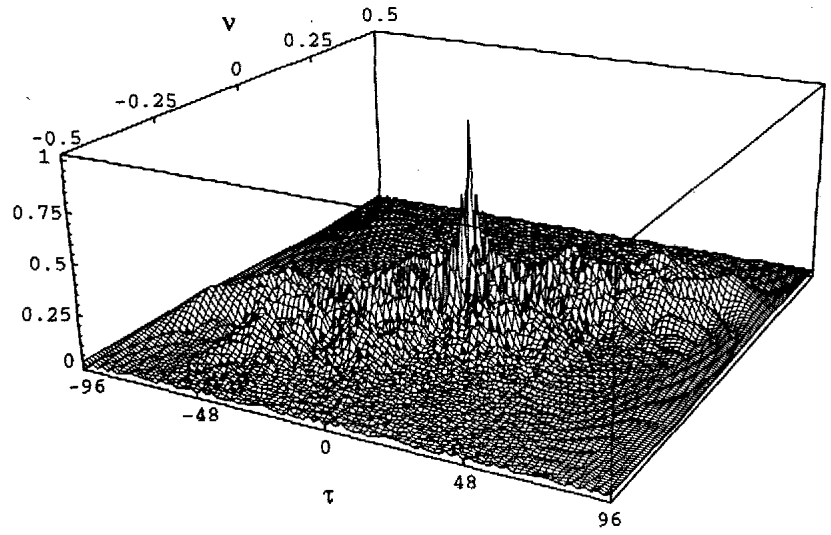

Fig. 19. Ambiguity surface of $s_0(t)$ in Table VII, $T = 16$.

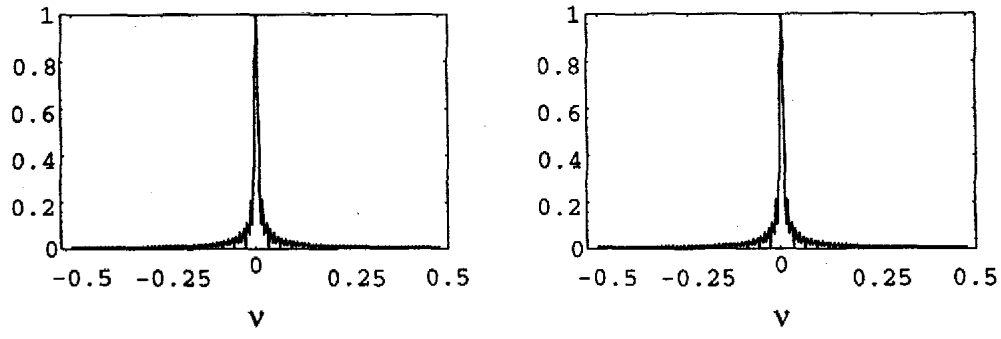

Fig. 20. Left: Cross cut of Fig. 19 at $\tau = 0$. Right: Cross cut of Fig. 18 at $\tau = 0$

V. Implementation

As mentioned in Section II, if the target environment cannot be exactly reproduced to allow the forming of multiple images using different point-spread functions, the multiple waveforms will have to be separated either in time slots or frequency channels. In this section we propose a time-division method for channel separation. Its frequency-domain duality can be obtained in a similar manner.

Suppose that the multiple signals are transmitted successively in time and that they are equally spaced by T, the pulse train can then be expressed as

$$s(t) = \sum_{n=0}^{N-1} s_n(t - nT).$$

If T is large enough so that there is no overlap between echoes of different pulses, a conventional pulse-Doppler radar

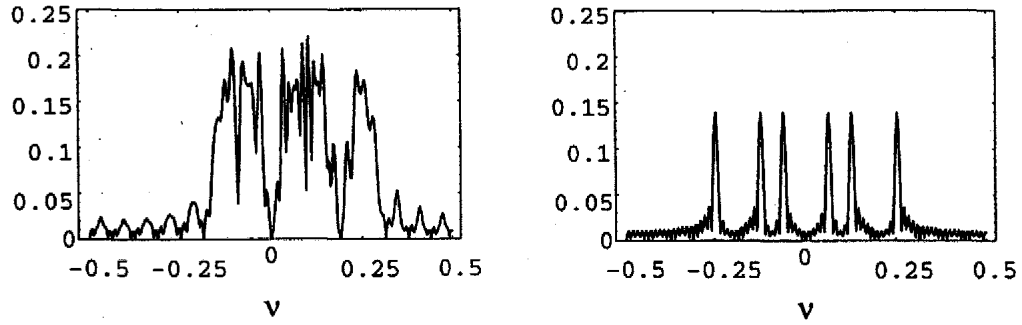

Fig. 21. Left: Cross cut of Fig. 19 at $\tau = T$. Right: Cross cut of Fig. 18 at $\tau = T$.

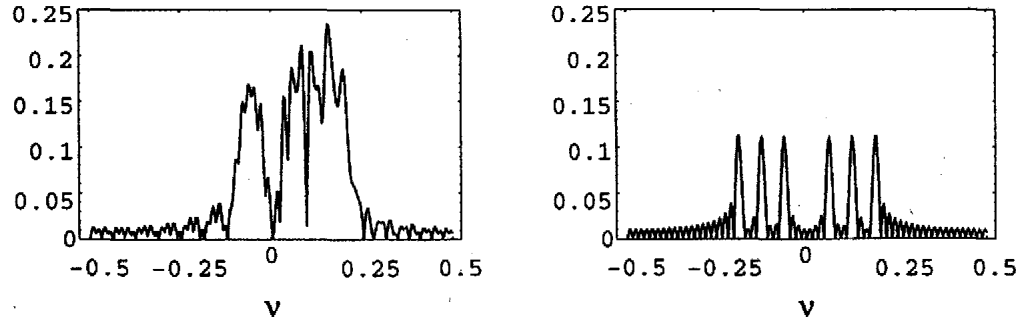

Fig. 22. Left: Cross cut of Fig. 19 at $\tau = 2T$. Right: Cross cut of Fig. 18 at $\tau = 2T$.

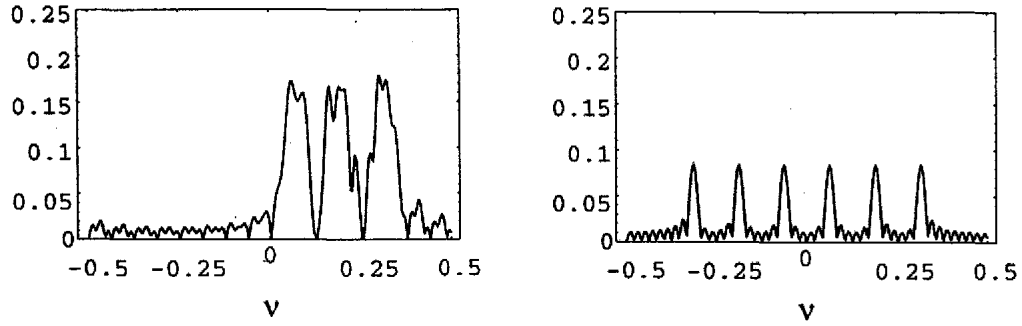

Fig. 23. Left: Cross cut of Fig. 19 at $\tau = 3T$. Right: Cross cut of Fig. 18 at $\tau = 3T$.

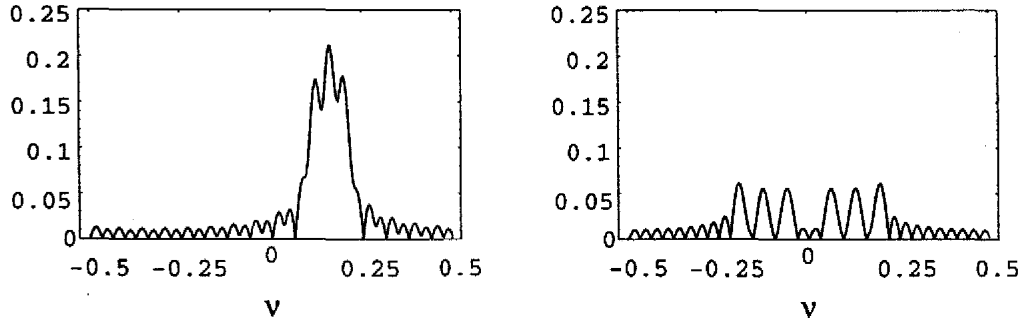

Fig. 24. Left: Cross cut of Fig. 19 at $\tau = 4T$. Right: Cross cut of Fig. 18 at $\tau = 4T$.

processor would consider $s(t)$ as a single waveform and match-filter the received signals over a time duration less than T in which the echoes are expected. As pointed out by Zeoli [15], this conventional processing method is actually equivalent to forming the targets' composite image using the CAF of $\{s_0(t), s_1(t-T), \cdots, s_{N-1}(t-(N-1)T)\}$. Since the ambiguity function of $s(t-nT)$ is $\exp\{-j2\pi\nu nT\}\chi_{s_n}(\tau, \nu)$, the radar images of a point target located at (τ_0, ν_0) corresponding to the individual waveforms are, as in (3),

$$\begin{aligned}
\mathcal{O}_T^0(\tau, \nu) &= \tilde{\chi}_{s_0}(\tau - \tau_0, \nu - \nu_0) \\
\mathcal{O}_T^1(\tau, \nu) &= e^{-j2\pi(\nu-\nu_0)T}\tilde{\chi}_{s_1}(\tau - \tau_0, \nu - \nu_0) \\
&\vdots \quad \vdots \\
\mathcal{O}_T^{N-1}(\tau, \nu) &= e^{-j2\pi(\nu-\nu_0)(N-1)T}\tilde{\chi}_{s_{N-1}}(\tau - \tau_0, \nu - \nu_0).
\end{aligned} \tag{15}$$

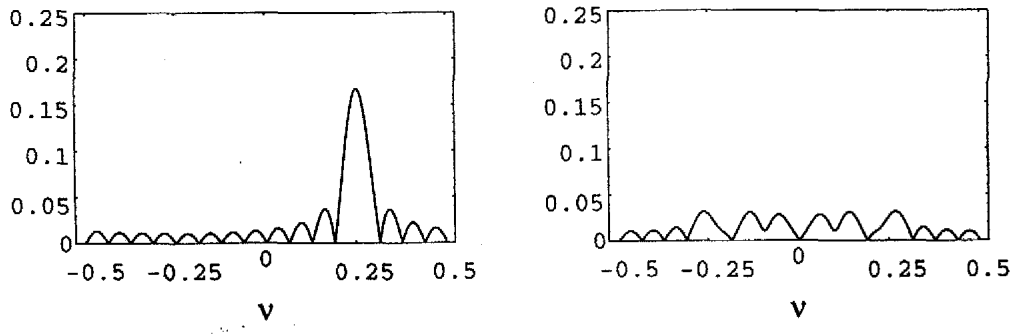

Fig. 25. Left: Cross cut of Fig. 19 at $\tau = 5T$. Right: Cross cut of Fig. 18 at $\tau = 5T$.

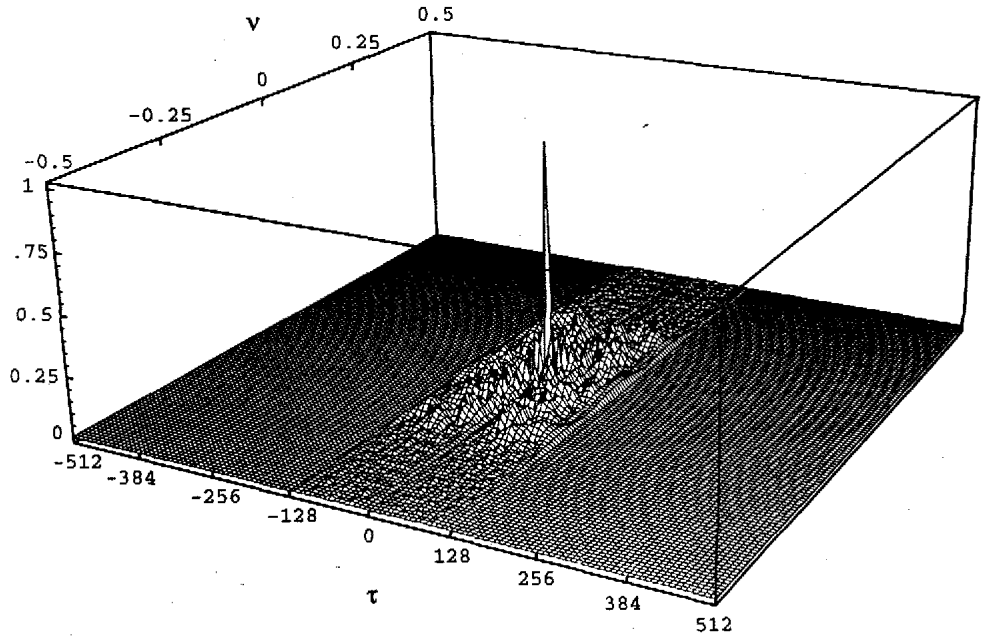

Fig. 26. CAF surface of signals in Table VIII, $T = 16$.

TABLE VIII
CODING PATTERN FOR A MIXED-FREQUENCY AND PHASE-MODULATED CODE

n		0	1	2	3	4	5	6	7	8	9	10	11	12	13	14	15
$s_0(t)$	$d_{0,n}$	1	4	3	7	7	2	0	6	6	0	2	7	7	3	4	1
	$\phi_{0,n}$	0				0				0				0			
$s_1(t)$	$d_{1,n}$	1	4	3	7	7	2	0	6	6	0	2	7	7	3	4	1
	$\phi_{1,n}$	0				$2\pi/4$				$4\pi/4$				$6\pi/4$			
$s_2(t)$	$d_{2,n}$	1	4	3	7	7	2	0	6	6	0	2	7	7	3	4	1
	$\phi_{2,n}$	0				$4\pi/4$				$8\pi/4$				$12\pi/4$			
$s_3(t)$	$d_{3,n}$	1	4	3	7	7	2	0	6	6	0	2	7	7	3	4	1
	$\phi_{3,n}$	0				$6\pi/4$				$12\pi/4$				$18\pi/4$			
$\psi_{i,n}(t) = P_T(t)$ for all i and n.																	

Note that for $\nu - \nu_0 = k \cdot 1/T$, where k is an integer, the modulating terms in (15) become one. Therefore, the CAF obtained by summing up the images in (15) is identical at these frequency values to that obtained by summing up the images in (3). Thus for the frequency-modulated codes described in Section IV-C, their sidelobe distributions remain the same even if the signals are staggered in time.

However, this is not the case for phase-modulated codes since the validity of these codes relies on the perfect alignment in both time and frequency at all values for exact sidelobe cancellation. Therefore, in order to use the phase-modulated codes, we must form the CAF of $\{s_0(t), s_1(t), \cdots, s_{N-1}(t)\}$ from the echoes of

$$\{s_0(t), s_1(t-T), \cdots, s_{N-1}(t-(N-1)T)\}.$$

To do this, let us consider the pulse train as N individual waveforms and define the impulse response of the matched filter for the nth waveform as

$$s(t - nT - \tau)\exp\{j2\pi\nu(t - nT)\}$$

as opposed to $s(t - nT - \tau)\exp\{j2\pi\nu t\}$ in pulse-Doppler processor. Equation (15) becomes

$$\begin{aligned}
\mathcal{O}_T^0(\tau, \nu) &= \tilde{\chi}_{s_0}(\tau - \tau_0, \nu - \nu_0) \\
\mathcal{O}_T^1(\tau, \nu) &= e^{j2\pi\nu_0 T}\tilde{\chi}_{s_1}(\tau - \tau_0, \nu - \nu_0) \\
&\vdots \quad \vdots \\
\mathcal{O}_T^{N-1}(\tau, \nu) &= e^{j2\pi\nu_0(N-1)T}\tilde{\chi}_{s_{N-1}}(\tau - \tau_0, \nu - \nu_0). \qquad (16)
\end{aligned}$$

It is now clear that in order to combine the images in the way described throughout the paper, i.e., forming the CAF of $\{s_0(t), s_1(t), \cdots, s_{N-1}(t)\}$, we need to estimate ν_0 and then co-phase the individual images by multiplying them by a complex factor $\exp\{-j2\pi\hat{\nu}_0 nT\}$ before summing them up together.

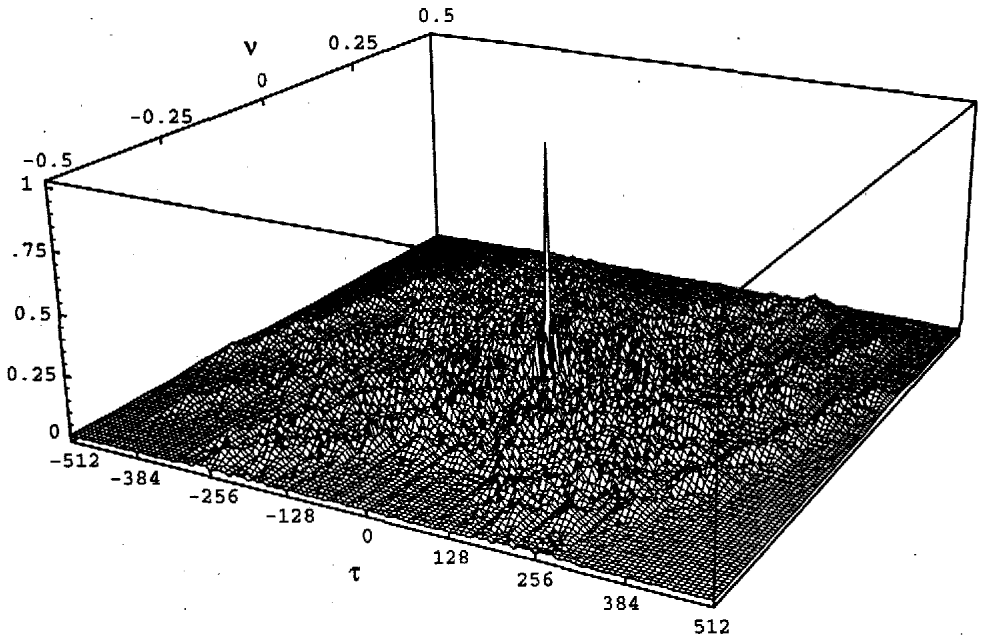

Fig. 27. Ambiguity surface of signal in Table II, $T = 16$.

As an example of using diverse waveform, consider microwave imaging in which the dynamic range of targets' reflectivities can be very large (60–90 dB). As a result it can be very difficult to differentiate between sidelobe returns of stronger targets and main lobe returns of weaker targets. Since the location of a stronger target can be accurately estimated, its CAF can be formed as discussed above, thus creating a "clean area" in which smaller targets cannot be hidden. Thus the weaker targets can be made visible if appropriate waveforms are chosen.

Note, however, that a second target located in (τ_1, ν_1) will be "out of focus" when the CAF of the first target is being formed since its image will be

$$\mathcal{O}_T^C(\tau, \nu) = \sum_{i=0}^{N-1} e^{j2\pi(\nu_1-\nu_0)iT} \chi_{s_i}(\tau - \tau_1, \nu - \nu_1) \quad (17)$$

unless $\nu_1 - \nu_0$ happens to be a multiple of $1/T$. However, its total energy on the $\tau - \nu$ plane does not go away as one can easily show that the ambiguity in (17) is the same as that of the focused image if the signals are orthogonal. It will then be detected and its parameters can be estimated by adjusting the focus of the imaging system.

A further complication may arise when the area being imaged contains several scatterers of high reflectivity. In this case it may be difficult to estimate the Doppler of one or more scatterers with sufficient accuracy. One possible approach to dealing with this problem is to use the best Doppler estimates available from the system and then perturb these estimates and iterate on them to increase discrimination by numerically maximizing the image contrast in a way similar to phase-correction procedures sometimes applied in synthetic-aperture radar. Even small residual errors from this type of procedure may make it impossible to detect smaller targets in the presence of the larger dominant scatterers. These problems will require further study in order to gain a full understanding of the possibilities of diversity waveform processing.

VI. Conclusion

In this paper, we have proposed a new method for obtaining enhanced discrimination delay-Doppler radar measurements using multiple waveforms. In our model, we assume that a radar can operate on several independent channels simultaneously, (i.e., it acts as if there are many radars observing the same target environment without interfering with each other). We then have the liberty of choosing the waveform for each channel. The analysis of this model leads to the introduction of the idea of composite ambiguity function of a signal set defined as the summation of the ambiguity functions of the signals in the set. By coherently combining the delay-Doppler images obtained by all individual channels, the resulting image can be considered as one obtained by using a point-spread function which is the composite ambiguity function of the set of the signals used by the different channels. Since the point-spread function determines the discrimination of a radar image, our attention is switched to the understanding of the composite ambiguity function.

A main theorem was then established to justify the superiority of this new point-spread function over the conventional point-spread function, which is the ambiguity function of the single transmitted waveform. This theorem states that for a set of signal with total energy E_T, its ambiguity defined as the volume under its associated composite ambiguity function can never be more than that of a single signal of the same energy. The same theorem also states that the minimum of this amount is the total energy E_T divided by the number of the signals and is achieved when the signal set is orthogonal and equal-energy.

With the main theorem serving as a general rule, we then study the design of signal sets for this new radar imaging

method. We are only interested in coded waveforms with constant amplitude. The families of constant-amplitude coded waveforms investigated in this paper include phase-coded waveforms, frequency-coded waveforms, and the mix of both. In phase-coded waveform design, we proposed a complementary code set that cancels all its sidelobes in both delay and Doppler; unlike the conventional complementary sequences that only cancel the sidelobes along zero-Doppler axis. In the case of frequency-coded waveforms, we introduced the notion of generalized Costas sequences, which contain the Costas sequences as a special case. At the cost of slightly increased signal bandwidth, the generalized Costas sequences provide an increased number of available sequences with distinct difference property over the Costas sequences alone. This enables us to find larger sets of sequences that have complementary sidelobe distributions. Also discovered in the frequency-coded waveform design is a set of circular Costas sequence with a sidelobe-distribution matrix that has a linearly decreasing peak-to-sidelobe ratio as τ increases. Finally, we took the advantage of both phase and frequency coding simultaneously to create a waveform set that has superior delay-Doppler discrimination characteristics to those of either phase or frequency coding alone. A practical implementation algorithm utilizing time-domain channel separation was also proposed to approximate the assumption of ideal coherent combining. For frequency-modulated codes, this time-division multiplexing method maintains the sidelobe distribution of the CAF. However, for phase-modulated codes, it requires additional complexity and may have more limited application.

REFERENCES

[1] T. P. Gill, *The Doppler Effect.* New York: Academic, 1965.

[2] A. W. Rihaczek, *Principles of High Resolution Radar.* New York: McGraw-Hill, 1969; Santa Monica, CA: Mark Resources, 1977.

[3] R. E. Blahut, "Theory of remote surveillance algorithms," *Radar and Sonar, Part I*, R. E. Blahut, W. Miller, and C. H. Wilcox, Eds. New York: Springer-Verlag, 1991.

[4] R. Sivaswami, "Self-clutter cancellation and ambiguity properties of subcomplementary sequences," *IEEE Trans. Aerosp. Electron. Syst.*, vol. AES-18, pp. 163–181, Mar. 1982.

[5] N. Sidiropoulos, J. Baras, and C. Bernstein, "Two-dimensional signal deconvolution using multiple sensors," in *Proc. Conf. Information Sciences and Systems* (Baltimore, MD, Johns Hopkins Univ., Mar. 20–22, 1991), pp. 594–599.

[6] T. Komatsu, T. Igarashi, K. Aizawa, and T. Saito, "Very high resolution imaging scheme with multiple different-aperture cameras," *Signal Processing: Image Commun.*, vol. 5, pp. 511–526, Dec. 1993.

[7] L. P. Yaroslavsky and H. J. Caulfield, "Deconvolution of multiple images of the same object," *Appl. Opt.*, vol. 33, no. 11, pp. 2157–2162, Apr. 10, 1994.

[8] J. W. Goodman, *Fourier Optics.* New York: McGraw-Hill, 1968.

[9] E. J. Kelly, "The radar measurement of range, velocity and acceleration," *IRE Trans. Mil. Electron.*, vol. MIL-5, pp. 51–57, Apr. 1961.

[10] W. L. Root, "Radar resolution of closely spaced targets," *IRE Trans. Mil. Electron.*, vol. MIL-6, pp. 197–204, Apr. 1962.

[11] W. Siebert, "A radar detection philosophy," *IRE Trans. Inform. Theory*, vol. IT-2, pp. 204–221, Sept. 1956.

[12] P. M. Woodward, *Probability and Information Theory, With Applications to Radar.* London, U.K.: Pergamon, 1953.

[13] L. Cohen, *Time-Frequency Analysis.* Englewood Cliffs, NJ: Prentice-Hall, 1995.

[14] M. Bernfeld, "Chirp Doppler radar," *Proc. IEEE*, vol. 72, pp. 540–541, Apr. 1984.

[15] G. W. Zeoli, "Comment on 'Self-clutter cancellation and ambiguity properties of subcomplementary sequences,' " *IEEE Trans. Aerosp. Electron. Syst.*, vol. AES-19, no. 5, pp. 780–781, Sept. 1983.

[16] R. Sivaswami, "On 'Comment on self-clutter cancellation and ambiguity properties of subcomplementary sequences,' " *IEEE Trans. Aerosp. Electron. Syst.*, vol. AES-22, pp. 97–98, Jan. 1986.

[17] M. J. E. Golay, "Complementary series," *IRE Trans. Inform. Theory*, vol. IT-6, pp. 400–408, 1960.

[18] K. Gerlach and F. F. Kretschmer, "General forms and properties of zero cross-correlation radar waveforms," *IEEE Trans. Aerosp. Electron. Syst.*, vol. 28, pp. 98–104, Jan. 1992.

[19] G. R. Welti, "Quaternary codes for pulsed radar," *IRE Trans. Inform. Theory*, vol. IT-6, pp. 400–408, June 1960.

[20] R. Turyn, "Ambiguity functions of complementary sequences," *IEEE Trans. Inform. Theory*, vol. IT-9, no. 1, pp. 46–47, 1963.

[21] Y. Taki, M. Miyakawa, M. Hatori, and S. Namba, "Even-shift orthogonal sequences," *IEEE Trans. Inform. Theory*, vol. IT-15, pp. 295–300, Mar. 1969.

[22] C. C. Tseng and C. L. Liu, "Complementary sets of sequences," *IEEE Trans. Inform. Theory*, vol. IT-18, pp. 644–652, Sept. 1972.

[23] R. Sivaswami, "Multiphase complementary codes," *IEEE Trans. Inform. Theory*, vol. IT-24, pp. 546–552, Sept. 1978.

[24] J. P. Costas, "A study of a class of detection waveforms having nearly ideal range-Doppler ambiguity properties," *Proc. IEEE*, vol. 72, no. 8, Aug. 1984.

[25] A. Freedman and N. Levanon, "Any two $N \times N$ Costas signals must have at least one common ambiguity sidelobe if $N > 3$—A proof," *Proc. IEEE*, vol. 73, pp. 1530–1531, Oct. 1985.

[26] O. Moreno, R. A. Games, and H. Taylor, "Sonar sequences from Costas arrays and the best known sonar sequences with up to 100 symbols," *IEEE Trans. Inform. Theory*, vol. 39, pp. 1985–1987, Nov. 1993.

[27] S. W. Golomb and H. Taylor, "Constructions and properties of Costas arrays," *Proc. IEEE*, vol. 72, Sept. 1984.

[28] S. W. Golomb, "Algebraic constructions for Costas arrays," *J. Comb. Theory*, ser. A, vol. 37, pp. 13–21, 1984.

[29] S. W. Golomb and O. Moreno, "On periodicity properties of Costas arrays and a conjecture on permutation polynomials," in *Proc. IEEE Int. Symp. Information Theory* (Trondheim, Norway, June 1994), p. 361.